Seismic evidence for the presence of Jurassic oceanic crust in the central Gulf of Cadiz (SW Iberian margin)

Valenti Sallarès, A. Gailler, Marc-André M-A Gutscher, David Graindorge, Rafael Bartolomé, Eulalia Gracia, Jordi Diaz, Juan José Dañobeitia, Nevio Zitellini

Seismic evidence for the presence of Jurassic oceanic crust in the central Gulf of Cadiz (SW Iberian margin)

Valentí Sallarès[(1,+)]

Audrey Gailler[(2,*)], Marc-André Gutscher[(2)], David Graindorge[(2)], Rafael Bartolomé[(1)], Eulàlia Gràcia[(1)], Jordi Díaz[(3)], Juan José Dañobeitia[(1)], Nevio Zitellini[(4)]

[(1)] Unitat de Tecnologia Marina-CSIC, Barcelona, Spain

[(2)] Université de Brest, Laboratoire Domaines Océaniques, UMR6538 CNRS/UBO, IUEM, Plouzané, France

[(3)] Institut de Ciencies de la Terra "Jaume Almera" (ICTJA), Solé i Sabaris, Barcelona, Spain

[(4)] Istituto di Scienze Marine (ISMAR)-CNR, Bologna, Italy

[(*)] now at Comissariat d'Energie Atomique, DAM/DIF, F-91297 Arpajon, France

[(+)] Corresponding author:

Valentí Sallarès

Unitat de tecnologia Marina (UTM)

Consejo Superior de Investigaciones Científicas (CSIC)

Passeig Marítim de la Barceloneta 37-49

08003 – Barcelona (Spain)

Email: vsallares@cmima.csic.es

Phone: +34 – 932 309 623

Fax: +34 – 932 309 555

Abstract

We investigate the crustal structure of the SW Iberian margin along a 340 km-long refraction and wide-angle reflection seismic profile crossing from the central Gulf of Cadiz to the Variscan continental margin in the Algarve, Southern Portugal. The seismic velocity and crustal geometry model obtained by joint refraction and reflection travel-time inversion reveals three distinct crustal domains: the 28-30 km-thick Variscan crust in the north, a 60 km-wide transition zone offshore, where the crust abruptly thins ~20 km, and finally a ~7 km-thick and ~150 km-wide crustal section that appears to be oceanic in nature. The oceanic crust is overlain by a 1-3 km-thick section of Mesozoic to Eocene sediments, with an additional 3-4 km of low-velocity, unconsolidated sediments on top belonging to the Miocene age, Gulf of Cadiz imbricated wedge. The sharp transition between continental and oceanic crust is best explained by an initial rifting setting as a transform margin during the Early Jurassic that followed the continental break-up in the Central Atlantic. The narrow oceanic basin would have formed during an oblique rifting and seafloor spreading episode between Iberia and Africa that started shortly thereafter (Bajocian) and lasted up to the initiation of oceanic spreading in the North Atlantic at the Tithonian (late Jurassic-earliest Cretaceous). The velocity model displays four wide, prominent, south-dipping low-velocity anomalies, which seem to be related with the presence of crustal-scale faults previously identified in the area, some of which could well be extensional faults generated during this rifting episode. We propose that this oceanic plate segment is the last remnant of an oceanic corridor that once connected the Alpine-Tethys with the Atlantic ocean, so it is, in turn, one of the oldest oceanic crustal fragments currently preserved on Earth. The presence of oceanic crust in the central Gulf of Cadiz is consistent with geodynamic models suggesting the existence of a narrow, westward retreating oceanic slab beneath the Gibraltar arc-Alboran basin system.

1. Introduction

The region offshore SW Iberia lies at the eastern end of the Azores-Gibraltar fracture zone (AGFZ), and is part of the complex plate boundary between the African and Eurasian plates (Figure 1). The tectonic behavior along the AGFZ is complex, varying from extensional in the West, close to the Mid-Atlantic Ridge, strike-slip in the center, along the Gloria fault, and mostly compressional in the East, from cape São Vicente to the Strait of Gibraltar. The regional tectonic history has been dominated by the long-term evolution of the triple junction between the North-American, African and Eurasian plates, as well as the interaction with other smaller blocks such as the Iberian plate (e.g. Srivastava et al., 1990; Olivet, 1996). Plate kinematic models and GPS observations show that Africa is currently moving in a NW-WNW direction with respect to Iberia at 4-5 mm/yr (Argus et al., 1989; Nocquet and Calais, 2004). This plate boundary is fairly diffuse, marked by an E-W trending band of seismicity about 100-200 km wide (e.g. Buforn et al., 1995). Moderate to strong earthquakes have struck here in the past, with a combination of compressional and strike-slip focal mechanisms (Grimison and Chen, 1986; Stich et al., 2003; 2006). In addition to this continuous, moderate magnitude seismic activity, the region has been also struck by large historical earthquakes, most notably the catastrophic Great Lisbon earthquake of 1755 (Mw=8.5-8.6) (Johnston et al., 1996).

A major limit exists in the Gulf of Cadiz between the Central Atlantic domain, which opened in the Early Jurassic, and the Northern Atlantic domain, which opened in the Upper Cretaceous (e.g., Roest and Srivastava, 1991; Olivet, 1996; Rovere et al., 2004; Sahabi et al., 2004). Available plate reconstruction models suggest that the region might have been the site of limited amounts of oceanic spreading due to the ESE migration of the African plate with respect to Iberia during this period of time (e.g. Stampfli and Borel, 2002; Schettino and

Turco, 2011). The possible presence of an oceanic basin of Jurassic age in this area is a largely debated question that has profound implications in the geodynamic evolution of the Western Mediterranean, and most specifically the Alboran basin system (e.g. Lonergan and White, 1997; Gutscher et al., 2002; Faccenna et al., 2004). Unfortunately, the nature of the crust in the deep oceanic domains offshore SW Iberia is unknown and difficult to determine because there are few recognizable magnetic anomaly patterns (Verhoef et al., 1991), and the seafloor is covered by a thick layer of Mesozoic to recent sediments, thus basement samples are difficult to obtain. The only deep sea drilling in the region that penetrated to the basement was the DSDP site 120 on Gorringe Bank (Figure 1), where serpentinized peridotite corresponding to exhumed mantle, gabbro, and extrusive rocks were sampled (Ryan et al., 1973). Similar rocks were also recovered during dredging and deep-sea submersible expeditions (Auzende et al., 1984; Girardeau et al., 1998). DSDP site 135 Southwest of the Coral Patch Ridge (Figure 1) penetrated Jurassic sediments (Aptian) but did not reach the basement (Hayes et al., 1972). Finally, continental rocks of Paleozoic age have been also sampled at the Guadalquivir Bank in the Iberian margin (Malod and Mougenot, 1979). Because of the lack of basement samples, current knowledge of the crustal domains in the Gulf of Cadiz is based almost exclusively on geophysical data. Available multi-channel seismic (MCS) data (Sartori et al., 1994; Banda et al., 1995; Torelli et al., 1997; Gràcia et al., 2006), as well as refraction and wide-angle reflection (WAS) data (Purdy, 1975; González et al., 1996; Gutscher et al., 2002) and models based on potential field data (e.g. Gràcia et al., 2003; Fullea et al., 2010), globally highlight the eastward increase in sediment thickness, depth to basement, and depth to Moho (Iribarren et al., 2007; Gutscher et al., 2009b), but do not provide information on the crustal nature across the different tectonic boundaries.

In fall 2008, in the framework of the EU-funded NEAREST (NEAR shore sourcES of Tsunamis: towards an early warning system) project, the NEAREST-SEIS WAS survey was

performed in the Gulf of Cadiz. During that survey, two long profiles using Ocean Bottom Seismometers (OBS) and land stations were acquired to probe the deep structure of the SW Iberian margin and adjacent oceanic areas (Figure 1). One of the profiles was mainly designed to shed light on the unresolved question of the crustal nature in the central Gulf of Cadiz (N-S profile in figure 1). The interpretation of the modeling results obtained along this profile, which begins in the Seine Abyssal Plain, crosses the Gulf of Cadiz imbricated wedge (GCIW) and several of the "SWIM" lineaments (Zitellini et al., 2009), the Portimao bank, and continues up onto the Portuguese continental shelf until the Variscan Iberian domain, are the main goals of the work presented in this paper.

2. Data acquisition

The WAS data were acquired onboard the Spanish R/V Hesperides. Fifteen OBS were deployed along a 257-km-long shooting line reaching from the southern tip of the GCIW into the Portimao Canyon (Figure 1). Four of the OBS were L-Cheapo 4x4 instruments, designed by the Scripps Institution of Oceanography, and belonging to the Spanish OBS pool operated by the UTM-CSIC. The other eleven OBS were from the joint IFREMER-IUEM pool (Auffret et al., 2004). The profile was extended on land in Portugal by 7 land-stations. Due to timing problems we used only 3 of these stations in the modelling, giving a total recording length of 342 km. The source was composed of 7 airguns organized in two arrays, providing a total volume of 4320 c.i. The arrays were deployed at a depth of 12 m, and the shot interval was set to 90 s (~210 m) to avoid noise generated by previous shots. Pre-processing of the OBS data included calculation of the clock-drift corrections and instrument relocation for spatial drift during their fall to the seafloor.

Most of the WAS data have a good quality, showing clear sedimentary (Ps) and intra-

crustal refracted phases (Pg), reflections at the sediment-basement interface (PsP) and crust-mantle boundary (PmP), and deeper arrivals refracted in the upper mantle (Pn) up to 100 km offset in some OBS, and to more than 150 km in the land stations. Five of the record sections at OBS and land stations are displayed in figure 2.

Seismic sections of the instruments located on the top of the GCIW show clear low-velocity sedimentary refractions (Ps) and reflections at the top of the basement (PsP). Significant variations are observed between record sections of the southern instruments, located towards the frontal part of the GCIW, and those located northward in the Algarve basin area (Figure 2d). Seismic sections from OBS located close to the Portimao canyon in very shallow water have limited quality. Conversely, long offset PmP and Pn phases can be clearly traced on the record sections of all the land stations (Figure 2e). Instruments located southward, in deeper water show clearer arrivals, including sediment and crustal arrivals (Figure 2a). In the modelling of the crustal structure we used data recorded at all the OBS and at the three land stations located the closest to the coast (Figure 1).

3. Travel-time picking and modelling approach

A total of 4003 picks, including first arrivals (Ps, Pg, Pn) and secondary reflections (PsP and PmP) were identified in the record sections. Picking was done manually on unfiltered data where possible and if needed, a deconvolution whitening, band-pass filtering (4-16 Hz) and Automatic Gain Correction were applied to improve lateral coherence and increase signal-to-noise ratio. Ps and PsP phases were observed and picked in all the OBS located on top of the sedimentary wedge, and Pg was also observed to variable offset in all the OBSs. PmP and Pn's could not be identified in all the record sections, especially in the two shallowest, northernmost OBSs. A picking uncertainty was assigned to the different picks

taking into account the quality of the phase, individual picking errors, and a possible systematic shift, of the order of half of the dominant period of the dominant signal, in the arrival identification. For Ps and near-offset Pg phases the average assigned uncertainty was 40-50 ms, while it was 60-70 ms for far-offset Pg's and 70-80 ms for Pn's. For PsP reflections it was 50-60 ms, and 70-80 ms for PmP's.

The 2-D velocity-depth model was obtained using the *tomo2d* joint refraction and reflection travel-time inversion code described in Korenaga et al. (2000). The method allows inverting simultaneously and independently travel-times from first arrivals and from a reflected phase, to obtain a velocity model and the geometry of a floating reflector. Travel-times and ray paths are calculated using a hybrid ray-tracing scheme based on the graph method (Moser et al., 1991) and a local ray bending refinement. Smoothing constraints for predefined correlation lengths and optimized damping for the model parameters are used to regularize the iterative linearized inversion (see Korenaga et al., 2000, for details).

To perform the inversion we employed an original multi-step, hybrid inversion strategy consisting of (1) splitting the data into two subsets, one for instruments located on the sedimentary wedge, and the other for those in the continental margin, and (2) adding the data sequentially, starting from the shortest offsets/uppermost levels, and finishing with the longest offsets/deepest levels.

The velocity model for the southern part of the profile was constructed in two steps, corresponding to the inversion of the sediments and crust. The Ps and PsP phases were used to invert for the velocities and thickness of the sedimentary wedge, and hence the geometry of the sediment-basement boundary (Figure 3a and 3b). The starting model was a laterally-extended "minimum 1-D velocity model", which is the one that fits the best the Ps travel-times (e.g. Sallarès et al., 2003). The top of the basement reflector was initially set at 7 km. The inverted velocity model of the sediments was included as a priori information in the

second inversion step, in which Ps, Pg and PmP arrivals were used to obtain the crustal velocity distribution and Moho geometry. The sediment velocity parameters were over-damped by a factor of 20 to 1 to let the inversion modify the model preferably within the crust. The starting velocity model below the sediment layer was a 1-D model varying uniformly from 4.5 km/s at the sediment-basement boundary to 7.2 km/s 7 km below, simulating an Atlantic oceanic crust older than 140 m.y. (White et al., 1992). The initial Moho reflector was set 7 km below the sediment-basement boundary. The corresponding 2-D crustal velocity model, obtained after 8 iterations, is shown in figures 3c and 3d.

The velocity model for the northern part of the profile was inverted in a single step, since no clear Ps or PsP phases were identified in the record sections. Consequently, sediments and crust were inverted together using the Pg and PmP phases to model the crustal velocity field and Moho geometry. The 2-D starting velocity model was constructed combining a 1-D model for the offshore section (i.e., the model that best fits Pg arrivals from the OBS located in the Algarve basin), and a second one for the onshore section, which was extracted from an onshore WAS profile acquired nearby (Palomeras et al., 2009). At the land-sea transition, the seismic velocities of the reference model were calculated by linear interpolation of these two 1-D velocity-depth models. The 2-D crustal velocity model for the northern section obtained after 8 iterations is shown in figures 3e and 3f.

In the third and last step, the southern and northern crustal models were merged together and a new inversion was performed using the whole set of refractions (Ps, Pg,and Pn) together with PmP's, to obtain a complete model including sediments, crust and uppermost mantle along the entire profile. As in the previous steps, the velocity nodes above the basal reflector were over-damped to favour model changes below the Moho. Beneath the Moho, a laterally-extended 1-D velocity-model with velocity varying uniformly from 7.5 km/s below the Moho to 8.3 km/s at 35 km depth, although alternative models with higher velocity

beneath the Moho were also tested. The 2-D velocity model obtained after 7 iterations is shown in figure 4. The final rms for this model is 65 ms (χ^2=1.02), with an rms of 61 ms for first arrivals and 72 ms for PmP's. The derivative weight sum (DWS), which is the column sum vector of the velocity kernel (Toomey and Foulger, 1989) and provides information on the linear sensitivity of the inversion, is shown in figure 5a.

4. Results

4.1. Seismic structure

The final velocity model in figure 4 shows marked differences between the sedimentary and crustal structures from south to north, with a marked transition zone between 160 and 210 km distance along the profile where the crust thins sharply. The southern part of the model (0-160 km along profile), which runs across the GCIW, shows a ~5 km thick layer corresponding to the sedimentary cover, with velocities ranging from ~1.8 km/s at the top to ~3.5 km/s at the base. This layer can in turn be subdivided in an upper layer of 2-3 km with velocity between ~1.6 km/s and 3.0 km/s, and a bottom one of 1-2 km with velocity between 2.8 km/s and 4.0 km/s. This sedimentary unit exhibits a quite uniform thickness along the southern 120 km of the profile, then thins progressively to the north, and more abruptly landward from ~125 km (between OBS37 and 38).

The crust below the sedimentary units shows a rather uniform thickness of ~7.0 km between 0 km and 160 km. Crustal velocities vary from 4.6-4.8 km/s at the top to 6.9-7.1 km/s at the base. The vertical velocity gradient is steeper in the uppermost crust (~0.45 s^{-1} in the upper 2 km) than in the lower part (~0.14 s^{-1} in the lower 5 km) (Figure 4). The Moho depth and geometry is constrained by PmP reflections, and it follows the basement topography along most of the section. The long-wavelength crustal velocity field is rather

225 uniform laterally, except for a pronounced anomaly centred at 130-145 km (between OBS38
226 and 39), as indicated by the depression of the velocity contours observed in this area (Figure
227 4) that gets down to the Moho but does not affect the sediments. The anomaly is clearly
228 imaged in figure 6 representing the negative anomalies with respect to a laterally-smoothed
229 velocity average along the profile. As it is observed in this figure, the corresponding anomaly
230 (f1) has an amplitude of -0.5 km/s, dips to the south, and is >10 km-wide. A second crustal-
231 scale low-velocity anomaly with similar geometry but lower amplitude (~-0.15 km/s) was
232 also detected at ~90 km (f0 in figure 6).
233 The profile section between 160 and 210 km (between OBS41 and 44) corresponds to
234 the rough topographic region between the GCIW and the Algarve Basin. This segment
235 accommodates almost all the crustal thickening. Within ~60 km, the Moho deepens from ~14
236 km to ~25 km depth (corresponding to a slope of ~12-13°), so the crust thickens drastically
237 from ~7 km to ~24 km. Northward from 210 km the vertical velocity gradient decreases
238 (~0.05 s^{-1}), reaching maximum velocities of 6.9-7.0 km/s just above the crust-mantle
239 boundary. The Moho geometry in this section is mainly constrained by PmP arrivals (OBS44
240 in figure 2d). The shallow velocity field at the transition zone from the oceanic domain
241 towards the continent indicates the presence of a thin sediment cover on top of the basement,
242 so that Ps/PsP phases are not distinguished in the record sections, so that the structure of the
243 sedimentary layers and the sediment-basement interface could not be properly defined. In this
244 area, two bathymetric highs are present, one located at ~180 km (the Portimao Bank) and the
245 other one located at 200-210 km (a spur bounding the Portimão canyon). The isovelocity
246 contour of 4.0 km/s reaches there almost the surface, indicating that the basement is possibly
247 outcropping here (BH in Figure 1). Two zones of relatively low crustal velocity, similar to
248 that described in the southern part of the model, can be seen at ~180-190 km (between OBS42
249 and 43) and ~225 km (around OBS44) (Figure 5). Both features are also reflected as

250 pronounced, south-dipping, negative velocity anomalies of up to -0.7 km/s that seem to start
251 at the seafloor and reach a maximum depth of 13-14 km (f2 and f3 in figure 6). Similarly to
252 f1, f2 and f3 extend laterally to >10 km in the model and show dip angles of 35-45º.
253 The northernmost part of the model, between 210 km and the end of the profile
254 (Figure 4), corresponds to the upper part of the contouritic drift and shelf and the Algarve
255 Basin, characterized by the Variscan basement. It shows only a residual sedimentary cover
256 that is less than 1 km-thick. In this area the Moho gently deepens from ~25 km at 210 km
257 along profile (between OBS43 and 44) to ~29 km at 260 km (north from OBS45 in figure 1).
258 A maximum crustal thickness of 29 km is obtained at the coastline, where crustal velocity
259 ranges from ~4.8 km/s and ~7.1 km/s. The velocity field in this area is mainly constrained by
260 the PmP phases recorded in the land stations, so there is a trade-off between lower crustal
261 velocity and Moho location. The upper mantle is sampled by Pn phases only a few kilometres
262 below the Moho, and the obtained velocity appears to be considerably low for upper mantle
263 (7.6-7.7 km/s).
264
265 ***4.2 Uncertainty analysis***
266 In order to estimate model parameters uncertainty owing to a combination of data
267 picking errors and other non-linear effects related to the theoretical approximations made, the
268 starting model selected, and the experiment geometry, we performed a Monte Carlo-type
269 stochastic error analysis. The approach followed is similar to that described in Sallarès et al.
270 (2005) and Gailler et al. (2007), which is a modified version of that of Korenaga et al. (2000),
271 and consists of: (1) generating a set of 250 2-D starting models by randomly perturbing
272 velocity and reflector depth in the initial models within reasonable bounds, which are chosen
273 according to *a priori* lithological information. In our case we have used the resulting model
274 shown in figure 4 as reference. Velocities have been varied within ±0.35 km/s in crust and

mantle, and Moho geometry within ±1.25 km in the oceanic domain and within ±2.5 km in the continent. In addition, 250 noisy data sets have been generated by adding random timing errors of ±60 ms, including common phase errors (±30 ms), common receiver errors (±10 ms), and individual picking errors (±20 ms), to the reference data set, constituted by first arrivals and PmPs. Then, we repeated the inversion for 250 randomly selected perturbed velocity models-noisy data set pairs, using the same inversion parameters as with the model shown in figure 4. According to Tarantola (1987), the mean deviation of all realizations of such an ensemble can be interpreted as a statistical measure of the model parameters uncertainty. The mean deviation of model parameters is shown in figure 5b. The average rms of all the Monte-Carlo realizations diminishes from 361 ms (χ^2=36.2) before the inversion, to 63 ms (χ^2=1.1) after the inversion.

Uncertainty within the sedimentary layer is low (≤0.1 km/s), increasing to ~0.15 km/s near the top of the basement, due to the sharp velocity contrast between sediments and basement and to the strong velocity gradient in the upper part of the crust (e.g. Calahorrano et al., 2008). Velocity uncertainty within the oceanic crust is also low (≤0.1 km/s), confirming that the crustal velocity field obtained in the oceanic domain of the model is remarkably well constrained by the data. The Moho geometry in this oceanic domain has an average uncertainty of less than ±0.5 km (Figure 5b).

The transitional and continental domains (between 160 km and the end of the model) also display rather low crustal velocity uncertainty, increasing from ≤0.15 km/s in average in the upper third of the crust to ~0.20 km/s near the Moho boundary. This locally high uncertainty reflects the lack of multi-fold ray coverage in this area, especially in the deep part of the model sampled only by PmP phases, which are subject to trade-off between the reflector location and the velocity field above it (e.g. Korenaga et al., 2000; Sallarès et al., 2005). Interestingly, Moho depth uncertainty in the continental domain is reasonably low,

varying between ±1.0 km in the transition zone, and ±1.5 km beneath the coast line, in the deepest part of the model (Figure 5b).

The worst-resolved part of the model corresponds to the upper mantle, where uncertainty is locally ≥0.2 km/s. A common problem in WAS experiments is that the low mantle velocity gradient makes that Pn phases do not dive deep into the mantle (see DWS plot in figure 5a), so they only carry limited information on the velocity structure of the uppermost few km of the mantle (e.g., Sallarès and Ranero, 2005). In order to test the reliability of the obtained upper mantle velocity, we performed two additional inversions using the same reference crustal velocity model and data set, but including two end-member uppermost mantle velocities of 7.4 km/s and 8.1 km/s. Both models converged to low mantle velocity ranging between ~7.5 km/s and ~7.8 km/s, respectively. Given that the upper mantle is covered only by Pn to a few km below the Moho, which have a very limited azimuthal coverage and have a limited penetration, the model parameter resolution at the upper mantle is low, so that the velocity represents an average along the ray path.

5. Discussion

5.1. Nature of the crustal domains offshore SW Iberia

The final velocity model of figure 4 reveals the presence two distinct crustal domains (labelled 1 and 2 in our interpretative model of figure 7, summarizing our main structural interpretations), with a transition zone in between. In domain 1 the crust is ~7.0 km thick. It is overlain by a 1-2 km of high-velocity sediments, and by other 3-4 km of lower-velocity sediments. These two sedimentary units had been previously identified in different local MCS profiles over the GCIW (Tortella et al., 1997; Torelli et al., 1997; Gràcia et al., 2003; Gutscher et al., 2009a). According to these authors the lower unit is constituted by Mesozoic

to Eocene sedimentary rocks, whereas the upper one includes the GCIW, mainly emplaced during Late Miocene, and a thin layer of Upper Miocene to plio-Quaternary sediments that overlay the GCIW. However, the interpretations regarding the evolution and tectonic behavior of both units differ in several aspects. A number of authors have suggested that the GCIW is an allocthonous body emplaced tectonically by the westward migration of the Gibraltar arc between ~15 Ma and ~8 Ma (e.g. Torelli et al., 1997; Gràcia et al., 2003; Medialdea et al., 2004; Iribarren, 2009), whereas Gutscher et al. (2009b) consider that this unit is as an actively deforming accretionary prism on top of an eastward-subducting oceanic slab, source of the largest earthquakes having occurred in the region. There is however overall agreement in that the lowermost unit covering the basement is Mesozoic in age (e.g. Sartori et al., 1993; Torelli et al., 1997; Tortella et al., 1997; Gràcia et al., 2003), giving an upper bound for the age of the basement below.

Domain 2 corresponds to the stable continental Variscan margin of SW Iberia, and consists of a continental crust (27-30 km thick) overlain by a poorly contrasted sedimentary layer made of Mesozoic units (Terrinha et al., 2003). The velocity structure and crustal thickness are very similar to that modelled along the on-shore IBERSEIS WAS transect (Palomeras et al., 2009), and it is also consistent with that of González et al. (1996), which is based on land recordings of the IAM data. The transition zone in between both domains is roughly 60 km-wide, across which occurs an abrupt lateral variation in crustal thickness between the continental margin and the central Gulf of Cadiz. The sharpest transition takes place at km 160-170 (marked by "COB" in figure 7).

Concerning the nature of the crust in domain 1, there are in principle three possible interpretations; namely thinned continental crust, exhumed mantle or oceanic crust. Available heat flow data above the GCIW indicate values from 59-45 mW/m^2 (Grevemeyer et al., 2008), values that are consistent with old lithosphere but do not help constraining the crustal

type. Some ENE-WSW trending magnetic anomalies are also present in the internal Gulf of Cadiz (Verhoef et al., 1991; Dañobeitia et al., 1999), but these are too subdued and sparse to be identified as seafloor spreading anomalies. In the absence of direct basement samples or well-defined magnetic anomalies, the best available indicator on the nature of the crust is the velocity structure and crustal thickness provided by offshore WAS data. Figure 8 shows a comparison of 1-D velocity-depth profiles representative of the two crustal domains and the transition zone with compilations made for: (1) exhumed mantle sections along the western Iberian margin (Srivastava et al., 2000), (2) >140 m.y.-old Atlantic oceanic crust (White et al., 1992), (3) continental crust (Christensen and Mooney, 1995), and (4) altered oceanic crust near subduction trenches (Meléndez et al., 2009). A comparison of the velocities obtained in domain 1 to velocities of exhumed/serpentinized upper mantle (Figure 8a) show that crustal velocities are far too slow and velocity gradients too smooth to correspond to exhumed mantle. In contrast, the obtained velocities are too high to correspond to extended continental crust (Figure 8a). An additional observation that helps to rule out this option of continental crustal affinity is that all the continental thinning occurs in domains 2 and 3, and there is no thinning at all in domain 1 for more than 150 km, an observation that is hardly compatible with an extended continental nature.

The comparison with the velocity structure for >140 m.y.-old Atlantic oceanic crust (White et al., 1992) is shown in figure 8b. The velocity structure in domain 1 is closer to oceanic crust than to the two options shown in figure 8a, but it is near the lower velocity bound. This atypical velocity profile may be the result of fault-related rock fracturing and subsequent alteration by fluids percolating through faults at this anomalously old (probably of Jurassic age, see introduction and explanation below), and hence cold and brittle crust. The presence of low velocity anomalies that spatially coincide with two of the long, N120°E trending strike-slip “SWIM lineaments”, interpreted by Zitellini et al. (2009) as crustal-scale

375 faults, would support this hypothesis. Anomaly f1 (figure 6) corresponds to the location of the
376 northernmost lineament (LN in figure 1), whereas f0 is located next to the southern one (LS in
377 figure 1). Additionally, the uppermost mantle velocity is low, which might be indicative of
378 mantle serpentinization, probably by means of fluids percolating through the aforementioned
379 faults crossing the Moho. The low crustal and upper mantle velocity is a common feature in
380 the oceanic plate at subduction zones. It has been described for the incoming plate in Chile
381 (Ranero and Sallarès, 2004; Lefeldt et al., 2009) and Middle America (Ivandic et al., 2009;
382 Meléndez et al., 2009). It has been associated to the presence of pre-existing lithospheric-
383 scale normal faults that are reactivated by flexure at the outer rise allowing the water to
384 percolate through the crust well into the upper mantle (Ranero et al., 2003). To check this
385 hypothesis, we have included in figure 8b a 1-D velocity-depth profile extracted from a WAS
386 profile acquired in the outer rise area of the Nicaraguan margin (Meléndez et al., 2009).
387 Clearly, this is the velocity profile that fits the best our model, suggesting that the crust in the
388 central Gulf of Cadiz could well be a fragment of fractured, altered and serpentinized oceanic
389 lithosphere. As expected, domains 2 and 3 (Figure 8c and 8d) show 1-D velocity-depth
390 profiles that fit well within the range of extended and normal continental crust velocities
391 (Christensen and Mooney, 1995). According to these observations continent-ocean boundary
392 (COB) is located at the northern limit of domain 1, some 100 km south from the coast line
393 (Figure 7).
394
395 ***5.2. Origin and tectonics of the SW Iberian and NW African margins***
396 The study area is located at the intersection of the NW African and the SW Iberian
397 continental margins. The NW African margin developed during Triassic-Jurassic times (Le
398 Roy and Piqué, 2001), as the Central Atlantic formed by the rifting of Africa from North
399 America at the southern end of the modern day Grand Banks of Newfoundland by extension

400 by transcurrent motion along the current southern Grand Banks fault (Bill et al., 2001;
401 Stampfli and Borel, 2002) (Figure 9). The SW Iberian margin and the Gulf of Cádiz domain
402 developed at the intersection of a N-S trending margin, between the West Iberia and the
403 Flemish Cap - Grand Banks Margin of Newfoundland (Canada), and the Grand Banks
404 transform referred to above (Roest and Srivastava, 1991). According to reconstructions based
405 on available plate tectonic models (Stampfli and Borel, 2002; Schettino and Turco, 2011) this
406 domain may have been the site of limited amounts of oblique seafloor spreading that
407 accommodated the ~N-S component of the migration of Africa with respect to Eurasia during
408 the Jurassic. This spreading could have opened a narrow oceanic basin separating southern
409 Iberia from NW Africa (Figure 9). These reconstructions indicate that the oceanic spreading
410 between Africa and Iberia would have been coeval with the opening of the Central Atlantic,
411 starting in the Bajocian (Middle Jurassic) at ~180 Ma (Roeser et al., 2002) and finishing with
412 the onset of rifting at the North Atlantic in the Tithonian (latest Jurassic), some 145 Ma
413 (Stampfli and Borel, 2002; Schettino and Turco, 2011).
414 Our work provides the first direct evidence for the presence of oceanic crust between
415 North Africa and SW Iberia. According to this interpretation, the oceanic crustal section
416 imaged in figure 4 would represent the westernmost segment of the Alpine-Tethys ocean, the
417 pre-Alpine oceanic domain that opened between NW Africa and Eurasia in the Jurassic and
418 closed during the Alpine orogeny (Stampfli and Borel, 2002; Schettino and Turco, 2011;
419 Handy et al., 2010). A south-eastern branch of this oceanic domain is the true Tethys, which
420 was consumed by north-dipping subduction as Africa converged northward with Europe, a
421 process which continues today beneath the Hellenic and Calabrian arcs (e.g. Faccenna et al.,
422 2001). Therefore, the Alpine-Tethys domain represented the boundary zone between the
423 Atlantic and Tethys domains during the Jurassic and the Mesozoic (Figure 9). According to
424 these reconstructions, the oceanic crustal segment that we have identified in the Gulf of Cadiz

would represent the last remnant of the western Alpine-Tethys lithosphere and, therefore, it would be one of the oldest oceanic crustal fragments currently preserved on Earth. It is interesting to note that the oceanic spreading would have mainly occurred during the so-called "Jurassic Quiet Zone" (Larson and Hilde, 1975), which would also explain the absence of a clear magnetic anomaly pattern in the area (e.g. Verhoef et al., 1991) despite its oceanic crustal nature.

In this context, we suggest that the large, prominent, south-dipping, low-velocity anomalies of figure 6 could be related with the presence of faults created during this rifting episode. Our interpretation is that they represent a smeared, coarse image of either the fractured, altered and fluid-saturated zone surrounding the fault area, or the contrast between rocks with different properties at both sides of the faults. According to our interpretation, f2 and f3 would correspond to extensional faults generated during this phase, whereas f1 (and possibly f0) could represent either normal faults created during oceanic spreading or fracture zones. As we explained above, f0 and f1 coincide spatially with the two northernmost "SWIM lineaments", whereas f2 coincides with a south-dipping fault reaching the seafloor that spatially coincides with the one imaged along MCS profile Voltaire-3 in the southern flank of the "Guadalquivir basement high" (see figure 9 in Terrinha et al., 2009). To our knowledge, there are no MCS data crossing the f3 anomaly (figure 6), so there is no link between this anomaly and other faults in the area. Finally, it is worth noting that f2 and f3 are imaged up to 13-14 km and no deeper, this is near the base of the upper crust in the Variscan belt (Palomeras et al., 2009). This depth corresponds to the maximum expected depth for continental earthquakes, which is believed to be associated with a thermal limit that marks the transition between "brittle" upper crust and "ductile" lower crust (e.g. Scholz, 1988).

5.3. Implications for regional geodynamic models

Different models have been proposed to date to explain the different geological, geophysical and geochemical observations of the Gibraltar arc-Alboran basin system, including past or present collision of continental lithosphere combined with lithospheric recycling either by convective removal (Platt and Vissers, 1989; Calvert et al., 2000), delamination (Seber et al., 1996), or slab break-off (Zeck, 1997); together with a variety of models of either continental or oceanic subduction with southward (Sanz de Galdeano, 1990; Morales et al., 1999), northward (Torres-Roldan et al., 1986; Mauffret et al., 2007), westward (Docherty and Banda, 1995; Zeck, 1997), or eastward dips (Lonergan and White, 1997; Gutscher et al., 2002). The nature of the crust in the Gulf of Cadiz has important implications for these competing geodynamic models proposed for the SW Iberia region, especially for those proposing rollback of an eastward dipping subducted slab as the main driving force for the formation of the Alboran basin (Lonergan and White, 1997; Gutscher et al., 2002; Duggen et al., 2004; Faccenna et al., 2004).

Some authors had previously suggested the presence a 10-15 km-thinning of the Variscan continental crust in the central Gulf of Cadiz, based on land recordings of marine seismic data (González et al., 1996), modelling of gravity data (Gràcia et al., 2003), combined modelling of potential field data (Fernández et al., 2004; Zeyen et al., 2005), and joint geophysical and petrological modelling (e.g. Fullea et al., 2010). In contrast, our current findings evidencing the presence of oceanic crust in the central Gulf of Cadiz are fully compatible with the presence of a narrow, east-dipping, fast retreating oceanic slab beneath the Gibraltar arc. Our model and interpretation is also in agreement with available seismological data suggest the presence of a continuous, 150-200 km-wide slab that dips from the Gulf of Cadiz towards Gibraltar, reaching the 660 km-discontinuity beneath the Alboran basin. These data include the global tomography images showing a narrow subducted slab beneath Alboran and Gibraltar (e.g. Spakman and Wortel, 2004), the dispersion analysis of

475 body waves from the deep mantle indicating the presence of a steeply eastward dipping low
476 P-wave waveguide within a high velocity slab (Bokelmann and Mauffroy, 2007), and the
477 recent shear-wave splitting measurements indicating a semicircular mantle flow pattern
478 beneath the Gibraltar arc (Díaz et al., 2010).
479
480 **6. Conclusions**
481
482 Our WAS modelling results indicate the presence of three crustal domains in the SW Iberian
483 margin. In the north, a 28-30 km-thick Variscan continental crust that gently thins to ~25 km
484 beneath the coastline. Immediately South from it, a ~60 km-wide zone where almost all the
485 crustal thinning (from ~25 km to ~7 km), concentrates. In the Southernmost part of the
486 profile, a 150 km-wide segment of ~7 km-thick crust, overlain by a 1-2 km-thick lower unit of
487 consolidated Mesozoic to Eocene sediments, and a 3-4 km-thick upper unit of sediments
488 corresponding to the Upper Miocene GCIW that is covered in turn by a thin layer of plio-
489 Quaternary sediments. The velocity gradient and crustal thickness in the southern section
490 strongly suggests that the lithosphere is oceanic in nature, although absolute velocities are
491 somewhat lower than "normal" probably due to fault-related rock fracturing and alteration
492 and mantle serpentinization. The abrupt ocean-continent transition is suggested to be the
493 result of the initial tectonics of the margin setting during the Triassic-early Jurassic as a
494 transform margin, followed by oblique seafloor spreading between southern Iberia and north-
495 western Africa during the Middle-Late Jurassic (roughly 180-145 Ma). According to our
496 interpretation, the oceanic spreading that took place in the Jurassic would have generated a
497 ~150 km-wide oceanic basin that would be part of the system that have once connected the
498 Atlantic and Tethyan oceanic domains. Based on the spatial coincidence with previously
499 identified active faults, we suggest that the wide, crustal-scale, south-dipping, low-velocity

anomalies imaged in the velocity model are the tomographic expression of the area affected by crustal-scale faults, some of which could have been created during this rifting period. The fragment of oceanic crust identified in the velocity model would therefore constitute the only remnant of the western Alpine-Tethys ocean and one of the oldest oceanic crustal fragments currently preserved on Earth. The presence of a narrow oceanic basin in the Gulf of Cadiz agrees with recent seismological observations, and it is consistent with the geodynamic models proposing roll-back of an eastward dipping slab as the main driving force for the opening of the Alboran Sea within the Betic-Rif system.

Acknowledgments

We thank the captain and crew of the research vessel BIO Hesperides, as well as the UTM and IFREMER technicians that were in charge of the airguns and OBS data acquisition. The NEAREST project has been funded by the the EU Programme "Integrating and Strengthening the European Research Area" of FP6, Sub-Priority 1.1.6.3, Global Change and Ecosystems", contract n. 037110, and the NEAREST -SEIS survey was funded by the Complementary Action # CGL2006-27098-E/ BTE of the Spanish MICINN. Additional funds were obtained from the MICINN project MEDOC (CTM2007-66179-C02-02/MAR). We also acknowledge funding from MICINN through the Ramon y Cajal programme (R. Bartolomé). We finally acknowledge the collaboration of our research partners at Grup de Recerca de la Generalitat de Catalunya Barcelona Centre of Subsurface Imaging (B-CSI) ref. 2009 SGR 146 and funding support from Repsol-YPF.

References

Argus, D.F., Gordon, R.G., Demets, C., Stein, S., 1989. Closure of the Africa-Eurasia-North America plate motion circuit and tectonics of the Gloria fault, J. Geophys. Res. 94, 5585-5602.

Auffret, Y., P. Pelleau, F. Klingelhoefer, J. Crozon, J.Y. Lin, and J. C. Sibuet, 2004. MicrOBS: A new ocean bottom seismometer generation. First Break, 22, 41-47.

Auzende, J. M., et al., 1984. Intraoceanic tectonism on the Gorringe Bank: Observations by submersible, in Ophiolites and Oceanic Lithosphere, edited by I. G. Gass, S. J. Lippard, and A. W. Shelton, Geol. Soc. Spec. Publ., 13, 113–120.

Banda, E., Torne, M., and the IAM Group, 1995. Iberian Atlantic Margins Group Investigates Deep Structure of Ocean Margins, a Multichannel Seismic Survey, EOS 76 (3), 25–29.

Bill, M., O'Dogherty, L., Guex, J., Baumgartner, P.O., Masson, H., 2001. Radiolarite ages in Alpine-Mediterranean ophiolites: Constraints on the oceanic spreading and the Tethys–Atlantic connection, Geol. Soc. Am. Bull., 113, 129–43.

Bokelmann, G. and Maufroy, E., 2007. Mantle structure under Gibraltar constrained by seismic waveform complexity, Geophys. Res. Let., 34, L22305, doi:10.1029/2007GL030964

Buforn, E., Sanz de Galdeano, C., and Udias, A., 1995. Seismotectonics of the Ibero-Maghrebian region, Tectonophysics, 248, 247-261.

Calahorrano, A., V. Sallarès, J.-Y. Collot, F. Sage and C. R. Ranero, 2008. Structure and physical properties of the subduction channel off the Gulf of Guayaquil (Ecuador) from seismic reflection data, Earth Planet. Sci. Lett., 267 (3-4), 453-467, doi:10.1016/j.epsl.2007.11.061

Calvert, A., Sandvol, E., Seber, D., Barazangi, M., Roecker, S., Mourabit, T., Vidal, F., Alguacil, G., and Jabour, N., 2000. Geodynamic Evolution of the Lithosphere and Upper Mantle Beneath the Alboran Region of the Western Mediterranean: Constraints from Travel Time Tomography, J. Geophys. Res., 105, 10,871-10,898.

548 Dañobeitia, J.J., Bartolome, R., Checa, A., Maldonado, A., and Slootweg, A.P., 1999. An
549 interpretation of a prominent magnetic anomaly near the boundary between the Eurasian and
550 African plates (Gulf of Cadiz, SW margin of Iberia). Marine Geology, 155, 45-62.
551 Diaz, J., J. Gallart, A. Villaseñor, F. Mancilla, A. Pazos, D. Córdoba, J.A. Pulgar , P. Ibarra, M.
552 Harnafi, and the TopoIberia Seismic Working Group, 2010. Mantle dynamics beneath the
553 Gibraltar Arc (W Mediterranean) from shear-wave splitting measurements on a dense seismic
554 array. Geophys. Res. Lett., 37 (18), L18304,doi: 10.1029/2010GL044201.
555 Docherty, C., and E. Banda, 1995. Evidence for the eastward migration of the Alboran Sea based on
556 regional subsidence analysis: A case for basin formation by delamination of the subcrustal
557 lithosphere?, Tectonics, 14 (4), 804–818, doi:10.1029/95TC00501.
558 Duggen, S., Hoernle, K., van den Bogaard, P., Harris, C., 2004. Magmatic evolution of the Alboran
559 Region: The role of subduction in forming the western Mediterranean and causing the Messinian
560 Salinity Crisis. Earth Planet. Sci. Lett. 218, 91-108.
561 Faccenna, C., Becker, T.W., Lucente, F.P., Jolivet, L. and Rossetti, F., 2001. History of subduction
562 and back-arc extension in the Central Mediterranean. Geophys. J. Int., 145: 809-820.
563 Faccenna, C., Piromallo, C., Crespo-Blanc, A., Jolivet, L. and Rossetti, F., 2004. Lateral slab
564 deformation and the origin of the western Mediterranean arcs. Tectonics, 23, 1-21.
565 Fernàndez, M., Marzan, I. and Torné, M., 2004. Lithospheric transition from the Variscan Iberian
566 Massif to the Jurassic oceanic crust of the Central Atlantic. Tectonophysics, 386, 97-115.Fullea,
567 J., Afonso, J.C., Fernàndez, M., and Vergés, J., 2007. A rapid method to map the crustal and
568 lithospheric thickness, using elevation, geoid and thermal analysis. Application to the Gibraltar
569 Arc System, Atlas Mountains and adjacent zones, Tectonophysics, 430, 97-117,
570 doi:10.1016/j.tecto.2006.11.003.
571 Fullea, J., Afonso, J. C., Fernàndez, M., Vergés, J., Zeyen, H., 2010. The structure and evolution of
572 the lithosphere - asthenosphere boundary beneath the Trans-Mediterranean region. Lithos, 120,
573 74-95, doi: 10.1016/j.lithos.2010.03.003.

574 Gailler, A., Charvis, P., and Flueh, E.R., 2007. Segmentation of the Nazca and South American plates
575 along the Ecuador subduction zone from wide-angle seismic profiles, Earth Planet. Sci. Lett.,
576 260, doi: 10.1016/j.epsl.2007.05.045.
577 Girardeau, J., G. Cornen, M.O. Beslier, B. Le Gall, C. Monnier, P. Agrinier, G. Dubuisson, L.
578 Pinheiro, A. Ribeiro, and H. Whitechurch, 1998. Extensional tectonics in the Gorringe Bank
579 rocks, eastern Atlantic ocean: Evidence of an oceanic ultra slow mantellic accreting centre, Terra
580 Nova, 10, 330–336.
581 González, A., Torné, M., Córdoba, D.,Vidal, N., Matias, L.M., Díaz, J., 1996. Crustal thinning in the
582 southwestern Iberia margin. Geophys. Res. Lett. 23, 2477–2480.
583 Gràcia, E., Danobeitia, J.J., Verges, J., Bartolome, R., 2003a. Crustal architecture and tectonic
584 evolution of the Gulf of Cadiz (SW Iberian margin) at the convergence of the Eurasian and
585 African plates. Tectonics 22, n.4, 1033, doi;10.1029/2001TC901045.
586 Gràcia, E., Danobeitia, J.J., Verges, J., PARSIFAL Team, 2003b. Mapping active faults offshore
587 Portugal (36°N-38°N): Implications for seismic hazard assessment along the southwest Iberian
588 margin. Geology, 31, 83-86.
589 Gràcia, E. and SWIM cruise party, 2006. Earthquake and Tsunami Hazards in the Southwest Iberian
590 Margin: High-resolution imaging of active faults and paleoseismic signature at the external part
591 of the Gulf of Cadiz . ESF EuroMargins SWIM Cruise Report (REN2002-11234-E-MAR), 46 pp
592 Grevemeyer, I., Kaul, N., and Kopf, A., 2008. Heat flow anomalies in the Gulf of Cadiz and off Cape
593 San Vicente, Portugal. Marine and Petroleum Geology, doi:10.1016/j.marpetgeo.2008.08.006.
594 Grimison, N. L., and W. P. Chen, 1986. The Azores□ Gibraltar plate boundary: Focal mechanisms,
595 depths of earthquakes, and their tectonic implications, J. Geophys. Res., 91(B2), 2029–
596 2047.Gutscher, M.-A., Malod, J., Rehault, J.-P., Contrucci, I., Klingelhoefer, F., Mendes-Victor,
597 L., Spakman, W., 2002. Evidence for active subduction beneath Gibraltar. Geology 30, 1071-
598 1074.
599 Gutscher, M.-A., Malod, J., Rehault, J.-P., Contrucci, I., Klingelhoefer, F., Mendes-Victor, L., and
600 Spakman, W., 2002. Evidence for active subduction beneath Gibraltar, Geology, 30, 1071– 1074

601 Gutscher, M.-A., Baptista, M.A., Miranda, J.M., 2006. The Gibraltar Arc seismogenic zone (part 2):
602 constraints on a shallow east dipping fault plane source for the 1755 Lisbon earthquake provided
603 by tsunami modeling and seismic intensity. Tectonophysics, Sp. Vol. "Natural laboratories on
604 seismogenic faults", v. 427, p. 153-166, doi:10.1016/j.tecto.2006.02.025.
605 Gutscher, M.-A., Dominguez, S., Westbrook, G., Gente, P., Babonneau, N., Mulder, T., Gonthier, E.,
606 Bartolome, R., Luis, J, Rosas, F., Terrinha, P., and the Delila and DelSis Scientific Teams.,
607 2009a. Tectonic shortening and gravitational spreading in the Gulf of Cadiz accretionary wedge:
608 observations from multi-beam bathymetry and seismic profiling. Journal of Marine and
609 Petroleum Geology, Sp. Vol. on Submarine instabilities. doi:10.1016/j.marpetgeo.2007.11.008.
610 Gutscher, M.-A., Dominguez, S., Westbrook, G.K., and Le Roy, P., 2009b. Deep structure, recent
611 deformation and analog modeling of the Gulf of Cadiz accretionary wedge: implications for the
612 1755 Lisbon earthquake. Tectonophysics Sp. Vol., Proc. of the MAPG Meeting Marrakech
613 Morocco (guest editor D. Frizon de Lamotte)., v. 475, p. 85-97, doi: 10.1016/j.tecto.2008.11.031.
614 Handy, M.R., Schmid, S., Bousquet, R., Kissling, E., Bernoulli, D., 2010. Reconciling plate-tectonic
615 reconstructions of Alpine Tethys with geological-geophysical record of spreading and
616 subductions in the Alps. Earth Sci. Rev., doi:10.1016/j.earscirev.2010.06.002.
617 Hayes et al., 1974, DSDP Site 135 (Survey report), DSDP Volume XIV, doi:10.2973/
618 dsdp.proc.14.1974
619 IOC, IHO and BODC, 2003. Centenary Edition of the GEBCO Digital Atlas, published on CD-ROM
620 on behalf of the Intergovernmental Oceanographic Commission and the International
621 Hydrographic Organization as part of the General Bathymetric Chart of the Oceans, British
622 Oceanographic Data Centre, Liverpool, UK.
623 Iribarren, L., Verges, J., Camurri, F., Fullea, J., Fernandez, M., 2007. The structure of the Atlantic-
624 Mediterranean transition zone from the Alboran Sea to the Horseshoe Abyssal Plain (Iberia –
625 Africa plate boundary). Marine Geology, 243, 97-119. doi:10.1016/j.margeo.2007.05.011.
626 Ivandic, M., Grevemeyer, I., Berhorst, A., Flueh, E. R. and McIntosh, K., 2008. Impact of bending
627 related faulting on the seismic properties of the incoming oceanic plate offshore of Nicaragua J.
628 Geophys. Res., 113 . B05410.

629 Johnston, A., 1996. Seismic moment assessment of earthquakes in stable continental regions - III New
630 Madrid 1811–1812, Charleston 1886 and Lisbon 1755. Geophys. J.Int. 126, 314–344.
631 Korenaga, J., W. S. Holbrook, G. M. Kent, P. B. Kelemen, R. S. Detrick, H. C. Larsen, J. R. Hopper,
632 and T. Dahl-Jensen, 2000. Crustal structure of the southeast Greenland margin from joint
633 refraction and reflection seismic tomography, J. Geophys. Res., 105, 21,591– 21,614
634 Larson, R. L., and T. W. C. Hilde, 1975. A Revised Time Scale of Magnetic Reversals for the Early
635 Cretaceous and Late Jurassic, J. Geophys. Res., 80 (17), 2586–2594, doi:10.1029/
636 JB080i017p02586.
637 Lefeldt, M., Grevemeyer, I., Goßler, J., and Bialas, J., 2009. Intraplate seismicity and releated mantle
638 hydration at the Nicaraguan trench outer rise, Geophys. J. Int., 178 (2), 742-752.
639 Le Roy, P., and Piqué, A., 2001. Triassic–Liassic western Moroccan synrift basins in relation to the
640 central Atlantic opening. Marine Geology, 172, 359–381,doi: 10.1016/S0025-3227(00)00130-4.
641 Lonergan, L. and N. White, 1997. Origin of the Betic-Rif mountain belt. Tectonics 16(3): 504-522.
642 Malod, J. A., and D. Mougenot, 1979. L'histoire géologique néogène du Golfe de Cadix, Bull. Soc.
643 Geol. Fr., XXI, 603 – 611.
644 Martinez-Solares, J.M., Lopez A., and Mezcua, J., 1979. Isoseismal map of the 1755 Lisbon
645 earthquake obtained from Spanish data. Tectonophysics 53, 301-313.
646 Mauffret, A., Ammar, A, Gorini, C., Jabour, H. 2007. The Alboran Sea (Western Mediterranean)
647 revisited with a view from the Moroccan Margin. Terra Nova, 19, 195–203.
648 Medialdea, T., Vegas, R., Somoza, L., Vázquez, J.T., Maldonado, A., Díaz-del-Rio, V., Maestro, A.,
649 Córdoba, D., Fernández-Puga, M.C., 2004. Structure and evolution of the "Olistostrome"
650 complex of the GibraltarArc in theGulf ofCadiz (eastern CentralAtlantic): evidence from two
651 long seismic cross-sections. Mar. Geol. 209, 173–198.
652 Meléndez, A., V. Sallarès, K. D. McIntosh, C. R. Ranero, 2009. Seismic structure of the Nicaraguan
653 convergent margin by travel time tomographic inversion of wide-angle seismic data in the area of
654 the 1992 Nicaragua slow earthquake, Abstract # T21C-1844, AGU General Meeting, San
655 Francisco (USA).

656 Morales, J., Serrano, I., Jabaloy, A., Galindo-Zaldívar, J., Zhao, D., Torcal, F., Vidal, F., González-
657 Lodeiro, F., 1999. Active continental subduction beneath the Betic Cordillera and the Alboran
658 Sea. Geology 27, 735–738.
659 Moser, T. J., 1991. Shortest path calculation of seismic rays: Geophysics, 56, 59–67.
660 Nocquet, J.M., and Calais, E., 2004. Geodetic measurements of crustal deformation in the Western
661 Mediterranean and Europe. Pure Appl. Geophys., 161, 661-681.
662 Olivet, J.-L., 1996. La cinématique de la Plaque Ibérique, Bull. Cent. Rech. Elf Explor. Prod., 20, 131-
663 195.
664 Palomeras, I., Carbonell, R., Flecha, I., Simancas, F., Ayarza, P., Matas, J., Martinez-Poyatos, D.,
665 Azor, A., González-Lodeiro, F., Pérez-Estaún, A., 2008. The Nature of the Lithosphere Across
666 the Variscan Orogen of SW-Iberia: Dense Wide-Angle Seismic Reflection Data. J. Geophys.
667 Res., 114, B02302, doi:10.1029/2007JB005050
668 Platt, J.P., and Vissers, R.L.M., 1989, Extensional collapse of thickened continental lithosphere: A
669 working hypothesis for the Alboran Sea and Gibraltar arc: Geology, v.17, p.540-543;
670 Purdy, G.M., 1975. The Eastern end of the Azores-Gibraltar plate boundary. Geophys. J. R. Astr. Soc.,
671 43, 123–150.
672 Ranero, C. R., Phipps Morgan, J., McIntosh, K., Reichert, C., 2003. Bending, faulting and mantle
673 serpentinization at the Middle America Trench. Nature, 425, 367-373.
674 Ranero, C. R. and Sallarès, V., 2004. Geophysical evidence for alteration of the crust and mantle of
675 the Nazca Plate during bending at the north Chile trench, Geology, 32 (7), 549-552
676 Roeser, H. A., C. Steiner, B. Schreckenberger, and M. Block, 2002. Structural development of the
677 Jurassic Magnetic Quiet Zone off Morocco and identification of Middle Jurassic magnetic
678 lineations, J. Geophys. Res., 107(B10), 2207, doi:10.1029/2000JB000094.
679 Roest, W. and Srivastava, S., 1991. Kinematics of the plate boundaries between Eurasia, Iberia, and
680 Africa in the North Atlantic from the Late Cretaceous to the present, Geology, 19, 613–616.
681 Rovere, M., Ranero, C.R., Sartori, R., Torelli, L., and Zitellini, N., 2004. Seismic images and
682 magnetic signature of Late Jurasic to Early Cretaceous Africa-Eurasia plate boundary off SW
683 Iberia. Geophysical Journal International, 158, 554-568.

Ryan et al., 1973. Gorringe Bank - Site 120 (Survey report), DSDP Volume XIII, doi:10.2973/dsdp.proc.13.1973

Sallarès, V., Ph. Charvis, E.R. Flueh and J. Bialas., 2003. Seismic structure of Malpelo and Cocos Volcanic Ridges and implications for hotspot-ridge interaction, J. Geophys. Res., 108, B12, 2564, doi: 10.1029/2003JB002431

Sallarès, V., Ph. Charvis, E. R. Flueh, J. Bialas and the SALIERI Scientific Party, 2005. Seismic structure of the Carnegie ridge and the nature of the Galapagos hotspot, Geophys. J. Int., 161 (3), 763-788, doi: 10.1111/ j.1365-246 X.2005.02592.x.

Sallarès, V. and C.R. Ranero, 2005. Structure and tectonics of the erosional convergent margin off Antofagasta, North Chile (23°30' S), J. Geophys. Res., 110, B6, 6101, doi: 10.1029/2004JB003418

Sanz de Galdeano, C., 1990. Geologic evolution of the Betic Cordilleras in the Western Mediterranean, Miocene to the present. Tectonophysics, 172, 107-119.

Sartori, R., Torelli, L., Zitellini, N., Peis, D., and Lodolo, E., 1994. Eastern Segment of the Azores-Gibraltar Line (Central-Eastern Atlantic): An Oceanic Plate Boundary with Diffuse Compressional Deformation, Geology, 22, 555–558.

Schettino, A., and Turco, E., 2011. Tectonic history of the western Tethys since the Late Triassic, Geol. Soc. Am. Bull., 123 (1/2); 89–105, doi: 10.1130/B30064.1

Scholz, C.H., 1988. The brittle-plastic transition and the depth of seismic faulting, Geol. Rundsch., 77 (1), 319-328.

Seber, D., Barazangi, M., Ibenbrahim, A., and Demnati, A., 1996. Geophysical evidence for lithospheric delamination beneath the Alboran Sea and Rif-Betic mountains. Nature, 379, 785-790.

Spakman, W. and Wortel, R., 2004 A tomographic view on Western Mediterranean Geodynamics. In: The TRANSMED Atlas. The Mediterranean region from crust to mantle. Geological and Geophysical framework. Cavazza, W., Roure, F., Spakman, W., Stampfli, G., and Ziegler, P. (Eds.) Episodes, 27, 31-52.

Srivastava, S.P., Schouten, H., Roest, W.R., Klitgord, K.D., Kovacs, L.C., Verhoef, J. and Macnab, R., 1990. Iberian plate kinematics: a jumping plate boundary between Eurasia and Africa. Nature, 344, 756-759.

714 Srivastava, S. P., Sibuet, J.-C., Cande, S., Roest, W.R. and Reid, I.D., 2000. Magnetic evidence for
715 slow seafloor spreading during the formation of the Newfoundland and Iberian margins. Earth
716 Planet. Sci. Lett., 182, 61-76.
717 Stampfli, G.M., and Borel, G.D., 2002. A Plate Tectonic Model for the Paleozoic and Mesozoic, Earth
718 Planet. Sci. Lett., 196 (1-2) 17-33.
719 Stich, D., Ammon, C.J., Morales, J., 2003. Moment-tensor solutions for small and moderate
720 earthquakes in the Ibero-Maghreb region. J. Geophys. Res. 108, 2148.
721 Stich, D., Serpelloni, E., Mancilla, F., Morales, J., 2006. Kinematics of the Iberia- Maghreb plate
722 contact from seismic moment tensors and GPS observations. Tectonophysics, 426, 295-317.
723 Stich, D., Mancilla F.d.L., Pondrelli S., Morales, J., 2007. Source analysis of the February 12th 2007,
724 Mw 6.0 Horseshoe earthquake : Implications for the 1755 Lisbon earthquake. Geophys. Res.
725 Lett., v. 34, L12308, doi :10.1029/2007GL030012.
726 Tarantola, A., 1987. Inverse problem theory: Methods for data fitting and model parameter estimation,
727 Elsevier Science, New York, 613 pp.
728 Terrinha, P., Pinheiro, L.M., Henriet, J.-P., Matia, L., Ivanov, A.K., Monteiro, J.H., Akhmetzhanov,
729 A., Volkonskaya, Cunha, M.R., Shaskin, P. and Rovere, M., 2003. Tsunamigenic-seismogenic
730 structures, neotectonics, sedimentary processes and slope instability on the Southwest Portugese
731 Margin. Marine Geology, 195, 55-73.
732 Terrinha, P., Matias, L., Vicente, J., Duarte, J., Luís, J., Pinheiro, L., Lourenço, N., Diez, S., Rosas, F.,
733 Magalhaes, V., Valadares, V., Zitellini, N., Mendes-Víctor, L. and MATESPRO Team, 2009.
734 Morphotectonics and Strain Partitioning at the Iberia-Africa plate boundary from multibeam and
735 seismic reflection data. Marine Geology, 267, 3-4, 156-174.
736 Thiebot, E., and Gutscher, M.-A., 2006. The Gibraltar Arc seismogenic zone (part1): constraints on a
737 shallow east dipping fault plane source for the 1755 Lisbon earthquake provided by seismic data,
738 gravity and thermal modeling. Tectonophysics Sp. Vol. “Natural laboratories on seismogenic
739 faults”, v. 427, p. 135-152, doi:10.1016/j.tecto.2006.02.024.
740 Toomey, D.R., and G.R. Foulger, 1989. Tomographic inversion of local earthquake data from the
741 Hengill-Grensdalur central volcano complex, Iceland, J. Geophys. Res., 94, 17,497-17,510.

742 Torelli, I., Sartori, R., Zitellini, N., 1997. The giant chaotic body in the Atlantic off Gibraltar: new
743 results from a deep seismic reflection survey. Marine and Petroleum Geol., 14, 125–138.
744 Torres-Roldan, R.L., Poli, G. and Pecerillo, A., 1986. An early Miocene arc-tholeiitic magmatic dyke
745 event from the Alboran Sea. Evidence for precollisional subduction and back-arc crustal
746 extension in the westernmost Mediterranean. Geol. Rundschau, 75 (1), 219-234.
747 Tortella, D., Torne, M., Perez-Estaun, A., 1997. Geodynamic evolution of the eastern segment of the
748 Azores–Gibraltar Zone: the Gorringe Bank and Gulf of Cadiz region. Marine Geophys. Res., 19,
749 211–230.
750 Verhoef, J., Collette, B. J., Danobeitia, J. J., Roeser, H. A., & Roest, W. R., 1991. Magnetic anomalies
751 off West-Africa, Mar. Geophys. Res., 13, 81-103.
752 White, R.S., McKenzie, D., O'Nions, R.K., 1992. Oceanic crustal thickness from seismic
753 measurements and rare earth element inversions. Journal of Geophysical Research, 97, 19683-
754 19715.
755 Zeyen, H., Ayara, P., Fernandez, M., and Rimi, A., 2005. Lithospheric structure under the western
756 African-European plate boundary: a transect across the Atlas Mountains and the Gulf of Cadiz.
757 Tectonics, 24, (TC2001), doi:10.1029/2004TC001639.
758 Zeck, H.P., 1997. Mantle peridotites outlining the Gibraltar Arc: Centrifugal extensional allocthons
759 derived from the earlier Alpine, westward subducted nappe pile. Tectonophysics, 281, 195–207
760 Zitellini, N., Rovere, M., Terrinha, P., Chierici, F., Matias, L., and BIGSETS Team 2004. Neogene
761 through Quaternary tectonic reactivation of SW Iberian passive margin. Pure Appl. Geophys.
762 161, 565-587.
763 Zitellini, N., Gràcia, E., Matias, L., Terrinha, P., Abreu, M.A., DeAlteriis, G., Henriet, J.P.,
764 Danobeitia, JJ., Masson, D., Mulder, T., Ramella, R., Somoza, L., and Diez, S., 2009. The quest
765 for NWAfrica-SW Eurasia plate boundary west of Gibraltar. Earth Planet. Sci. Lett. v. 280, p. 13-
766 50, doi :10.1016/j.epsl.2008.12.005.
767

Figure Captions

Figure 1.- Location map of the study area of the NEAREST-SEIS wide-angle seismic survey, including the two profiles that were acquired. Yellow circles display OBS and land stations locations along the N-S profile presented in this paper. The multi-beam bathymetry is a combination of the SWIM compilation (Zitellini et al., 2009) and GEBCO digital atlas (IOC et al., 2003). The different faults are taken from the NEAREST active faults map (Zitellini et al., 2009). White stars mark the location of DSDP sites 120 and 135. Inset: Global map including the major tectonic plates. Abbreviations: AB: Alboran Basin; AGFZ; Açores-Gibraltar Fault Zone; EUR: Eurasian plate, AFR: Africa/Nubia plate, IB: Iberia, BH: Basement High; CPS: Coral patch ridge, CPRF: Coral Patch Ridge fault, GF: Gloria Fault; GO: Gorringe bank, HAP: Horseshoe Abyssal Plain, HF: Horseshoe fault, LN: North SWIM lineament, LS: South SWIM lineament, PC: Portimao Canyon; SAP. Seine Abyssal plain, TAP: Tagus Abyssal Plain.

Figure 2.- Recorded seismic sections (up) and record sections with corresponding observed arrivals (grey circles with error bands) and calculated arrivals (white circles), corresponding to the vertical component of OBS32 (a), OBS37 (b), OBS41 (c), OBS44 (d) and lans station # 3 (d). Their corresponding locations along the profile can be seen in figure 1. The vertical axis represents reduced travel time (in seconds), and the vertical axis is offset (in km). Reduction velocity is 6 km/s. The white labels indicate the seismic phases that have been identified and modelled (see text for description). Short data gaps (white bands) are present in 3 OBS and the land station.

Figure 3.- Partial results at the different steps of the tomographic inversion procedure and ray tracing corresponding to the inverted seismic phases. White circles indicate OBS locations. Grey lines show the different geological boundary interfaces. (a) Resulting velocity model for the sedimentary layer. (b) Ray coverage of seismic phases used in the sedimentary layer inversion (Ps, PsP). (c) Resulting velocity model for the oceanic crust segment. (d) Ray coverage of seismic phases used in the oceanic crust inversion (Ps, Pg, PmP). (e) Resulting velocity model for the continental crust. (f) Ray coverage of seismic phases used in the continental crust inversion (Pg, PmP).

Figure 4.- 2-D final velocity model obtained by tomographic inversion of the whole data set, constituted by arrival times of Ps, PsP, Pg, PmP and Pn phases. White circles indicate OBS locations. Black lines show the sediment-basement and crust-mantle boundaries (i.e., Moho). The initial model used in the inversion is a combination of the models displayed in figure 3 (see text for details).

Figure 5.- (a) Derivative weight sum (DWS), and (b) Velocity and Moho depth uncertainty corresponding to the mean deviation of the 250 Monte Carlo realizations (see text for details). White circles indicate OBS locations.

Figure 6.- Map of negative velocity anomalies along the velocity profile, which correspond to the difference between the model displayed in figure 4 and a laterally-smoothed version of the same model. The filter applied to smooth the model is a Gaussian one with a lateral correlation length of 20 km and a vertical correlation length of 0.5 km. f0, f1,f2, and f3 indicate the location of the most prominent and continuous features in the model that are interpreted in the text. White circles indicate OBS locations.

816

817 **Figure 7.-** Interpretative model of the structure and tectonics of the SW Iberian margin along
818 the WAS profile displayed in figure 1. The different units and domains discussed in the text
819 are indicated with the different colors. White circles indicate OBS locations. Abbreviations:
820 f0, f1,f2, and f3 are faults; COB: Continent-Ocean Boundary, GCIW: Gulf of Cadiz
821 imbricated wedge; LC: Lower Crust; UC: Upper Crust; BH: Basement High.

822

823 **Figure 8.-** 1-D P-wave velocity/depth profiles shown at three different locations along the
824 WAS profile compared with compilations made for exhumed mantle, oceanic crust, and
825 continental crust. (a) 1-D velocity-depth profile extracted at 60 km along the profile (P2,
826 black line) and corresponding uncertainty bar (grey band), velocity profiles of exhumed
827 mantle sections along the western Iberian margin (Iap, green line) and Tagus Abyssal plain
828 (Tap, yellow line) (Srivastava et al., 2000), extended continental crust (ECC, brown area)
829 (Christensen and Mooney, 1995), (b) 1-D velocity-depth profile extracted at 60 km along
830 profile (P2, black line) and corresponding uncertainty bar (grey band), velocity profiles from
831 Atlantic oceanic crust older than 140 m.y. (AOC, blue area) (White et al., 1992) and
832 fractured, altered oceanic crust and serpentinized mantle at the outer rise of the Nicaragua
833 subduction zone (FOC, dark blue line with error band) (Meléndez et al., 2009), (c) 1-D
834 velocity-depth profile extracted at 190 km along profile (P2, black line) and corresponding
835 uncertainty bar (grey band), velocity profiles from AOC and ECC (see definition above), (d)
836 1-D velocity-depth profile extracted at 190 km along profile (P2, black line) and
837 corresponding uncertainty bar (grey band), velocity profiles from non-extended continental
838 crust (CC, brown area) (Christensen and Mooney, 1995).

839

840 **Figure 9.-** Sketch summarizing our interpretation of the geodynamic and tectonic evolution
841 between Eurasia/Iberia, Africa and north America during the Jurassic. The sequence includes
842 (a) the initial phase of the ~E-W oceanic spreading at the Central Atlantic and the opening of
843 the fracture zone, and (b) the initiation of oceanic spreading between Iberia and Africa to
844 generate a series of narrow oceanic basins of oceanic crust connecting the Tethyan and
845 Atlantic domains. Abbreviations: Bal: Balearic islands; Sar: Sardegna; Cor. Corsica; Adr:
846 Adriatic; Apul: Apulia; Kab: Kabilie.

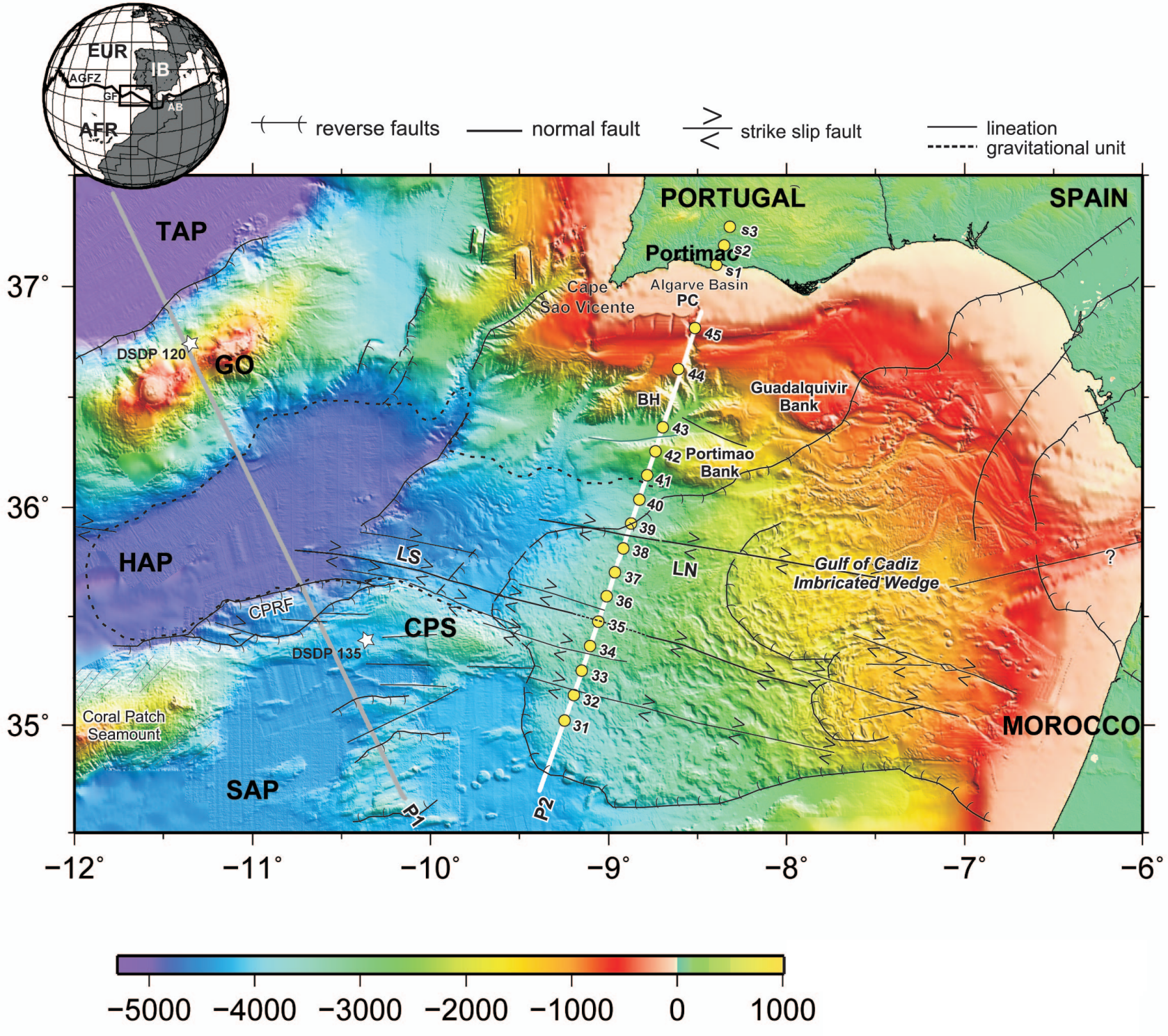
EUR
IB
AGFZ
GF
AB
AFR
reverse faults
normal fault
strike slip fault
lineation
gravitational unit
PORTUGAL
SPAIN
MOROCCO
TAP
HAP
SAP
GO
CPS
LS
LN
CPRF
BH
PC
Portimao
s3
s2
s1
Cape
Sao Vicente
Algarve Basin
Guadalquivir
Bank
Portimao
Bank
Gulf of Cadiz
Imbricated Wedge
DSDP 120
DSDP 135
Coral Patch
Seamount
P1
P2
45
44
43
42
41
40
39
38
37
36
35
34
33
32
31
37°
36°
35°
−12°
−11°
−10°
−9°
−8°
−7°
−6°
−5000
−4000
−3000
−2000
−1000
0
1000

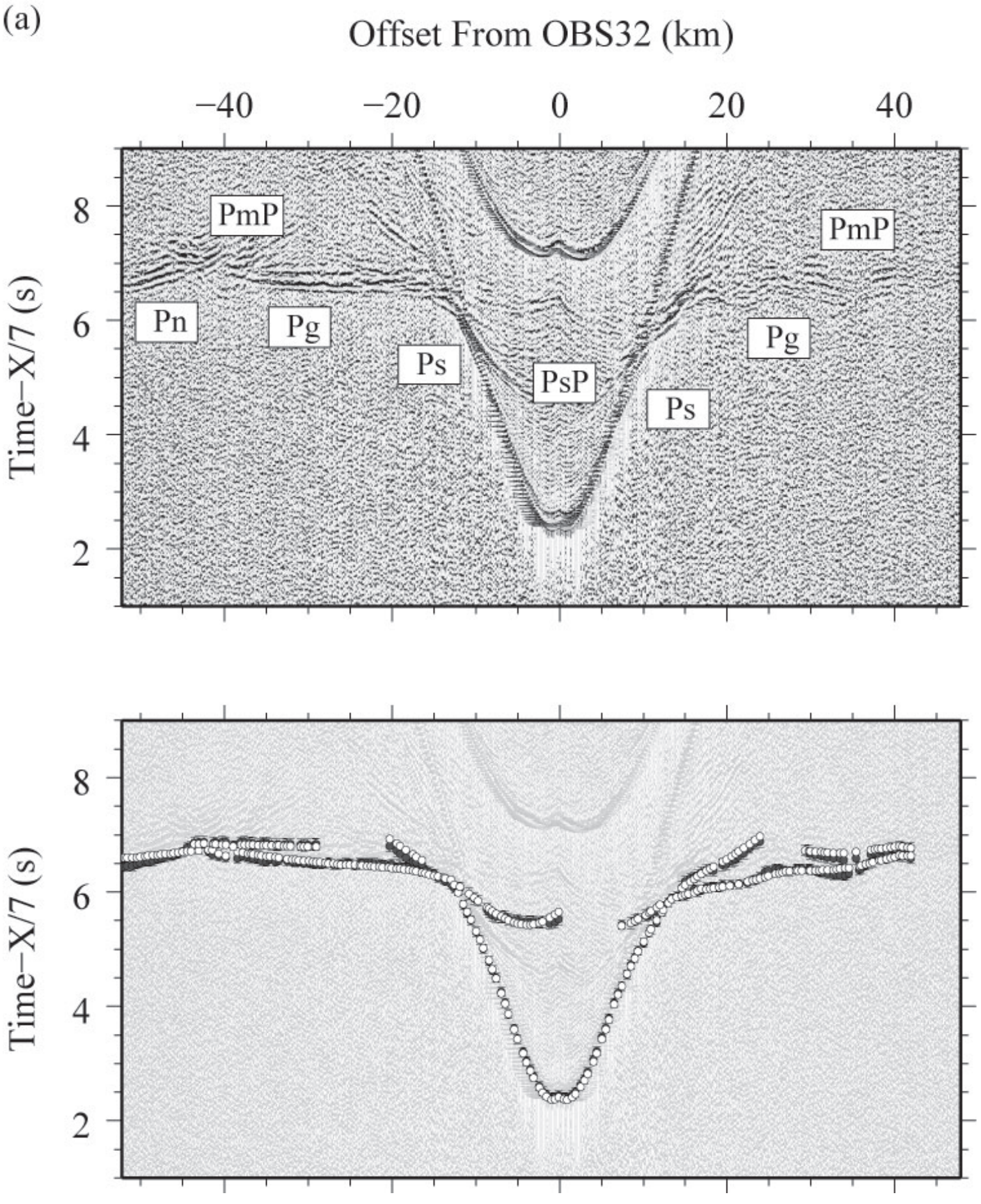
(a)
Offset From OBS32 (km)
−40
−20
0
20
40
Time−X/7 (s)
8
6
4
2
PmP
Pn
Pg
Ps
PsP
Ps
Pg
PmP
Time−X/7 (s)
8
6
4
2

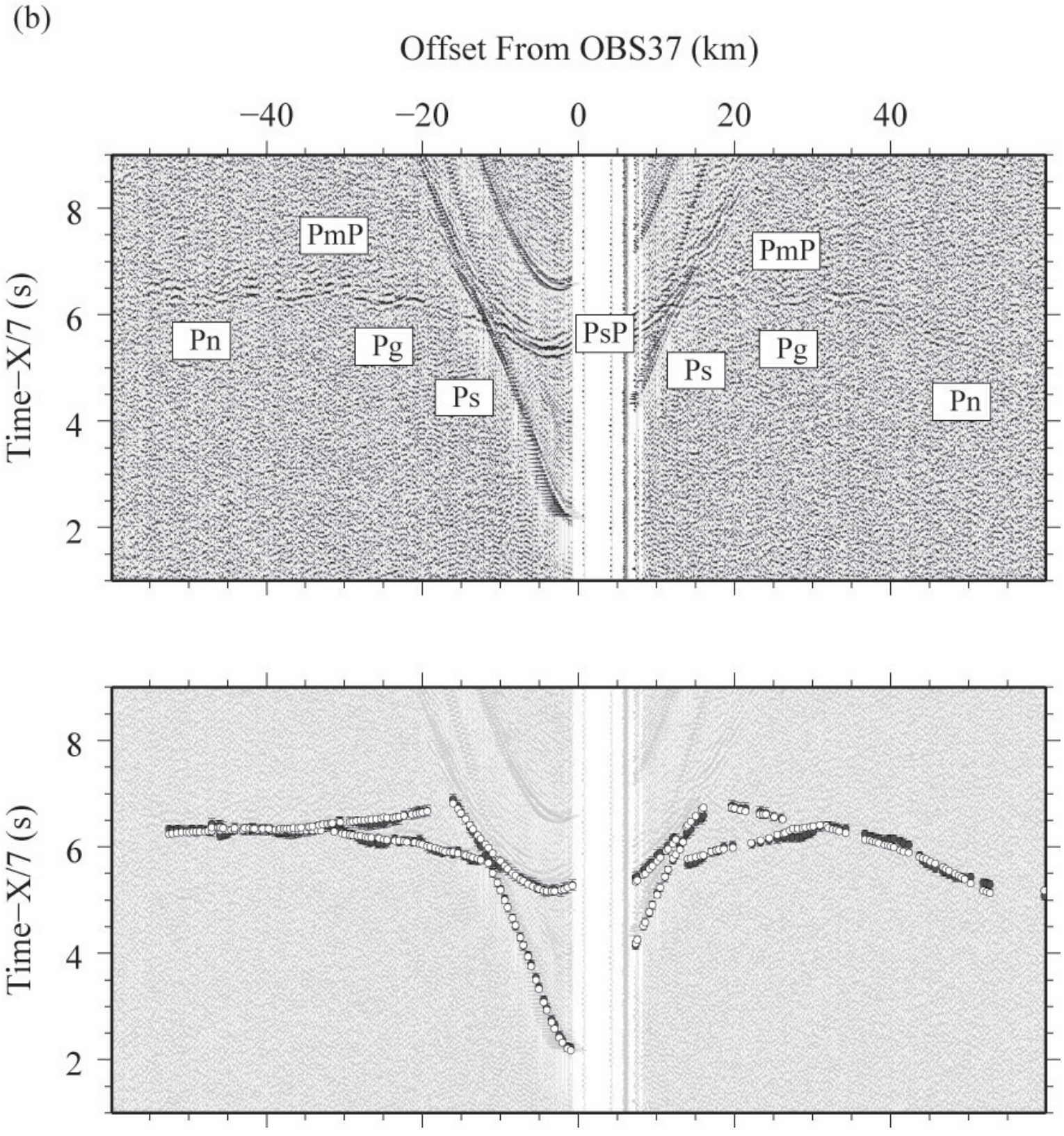
(b)
Offset From OBS37 (km)
−40
−20
0
20
40
Time−X/7 (s)
8
6
4
2
PmP
Pn
Pg
Ps
PsP
PmP
Ps
Pg
Pn
Time−X/7 (s)
8
6
4
2

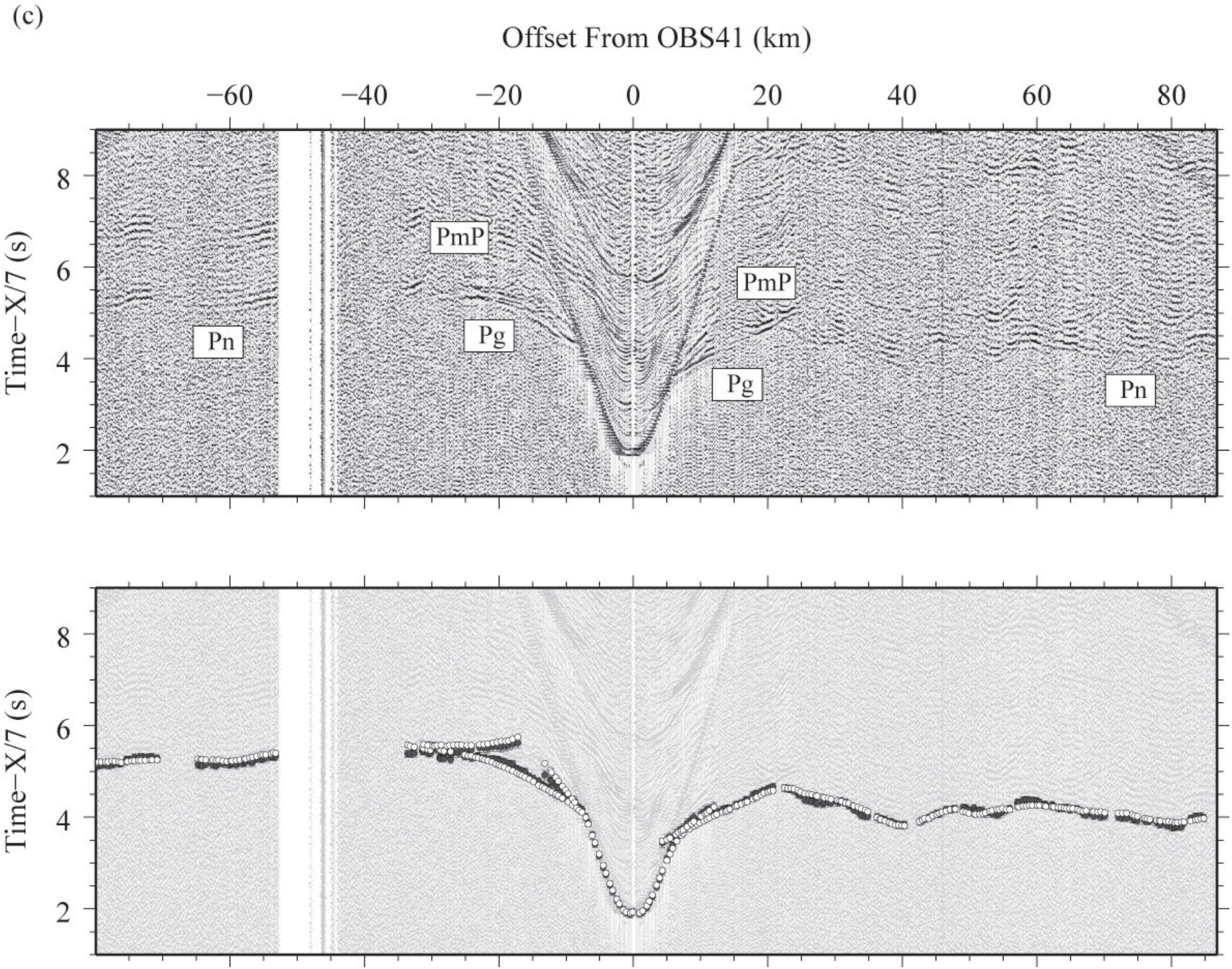
(c)
Offset From OBS41 (km)
−60
−40
−20
0
20
40
60
80
Time−X/7 (s)
8
6
4
2
Pn
PmP
Pg
PmP
Pg
Pn
Time−X/7 (s)
8
6
4
2

(d)

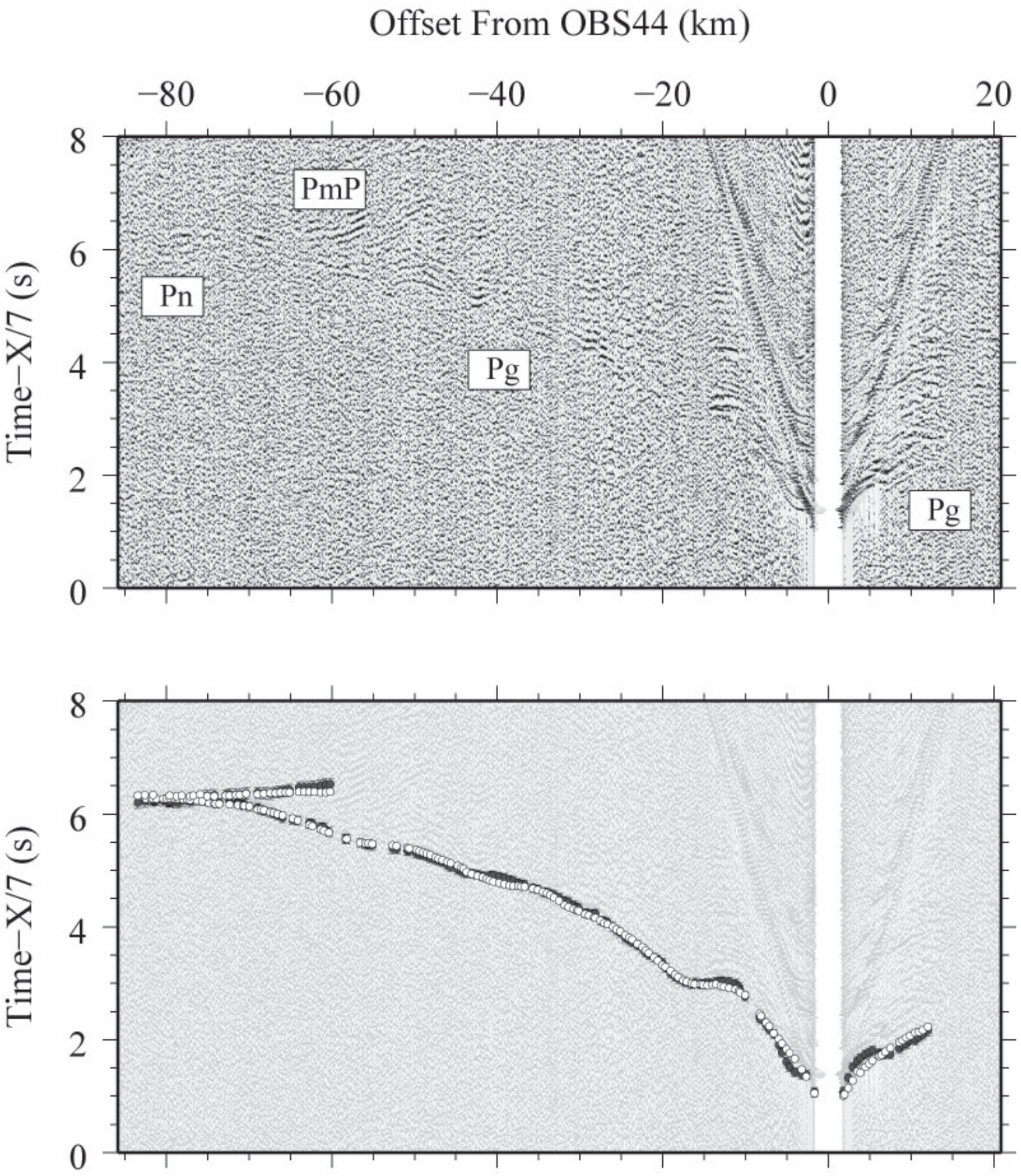
Offset From OBS44 (km)
−80
−60
−40
−20
0
20
8
6
4
2
0
Time−X/7 (s)
PmP
Pn
Pg
Pg
8
6
4
2
0
Time−X/7 (s)

(e)

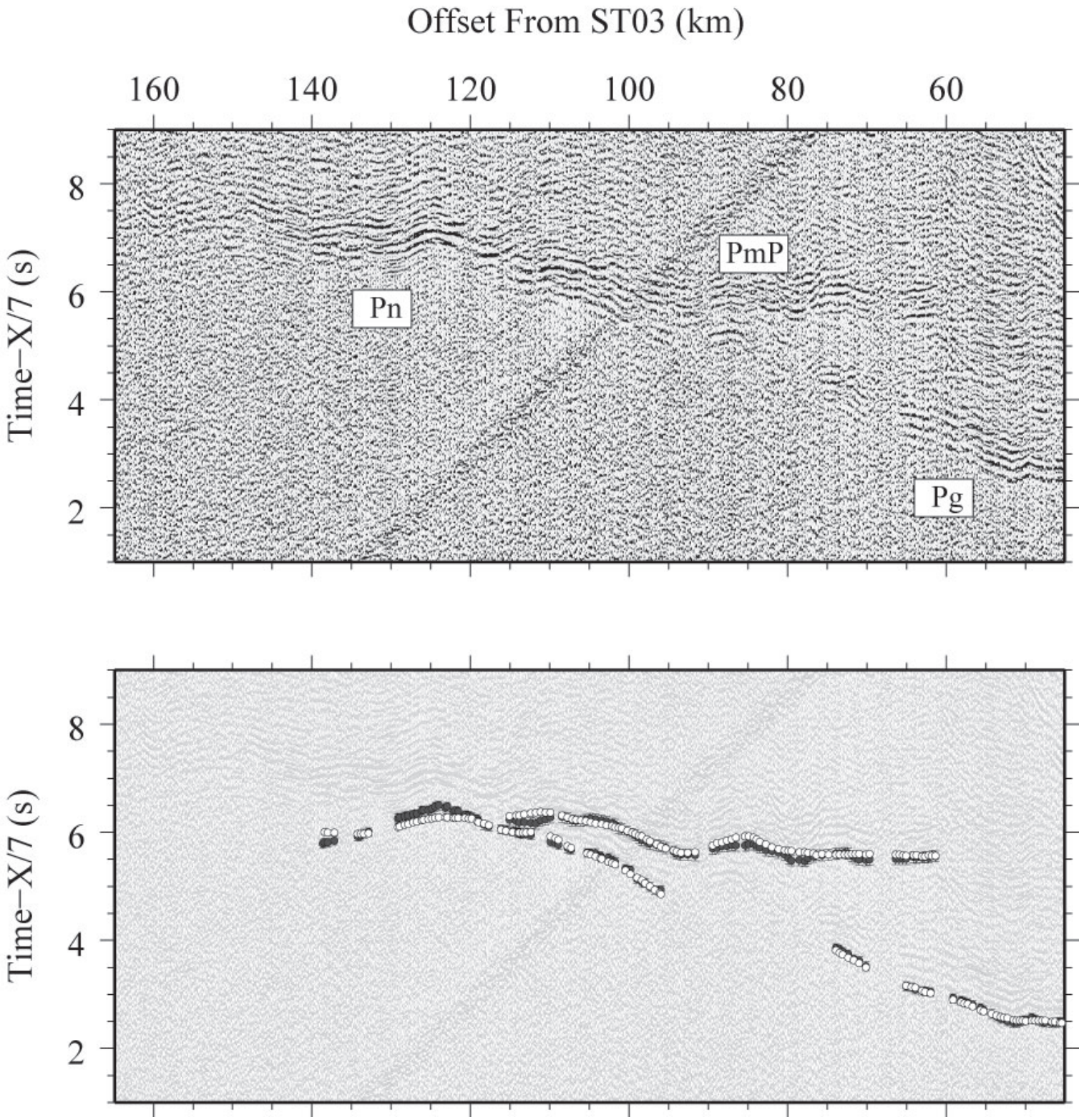
Offset From ST03 (km)
160
140
120
100
80
60
Time−X/7 (s)
8
6
4
2
Pn
PmP
Pg
Time−X/7 (s)
8
6
4
2

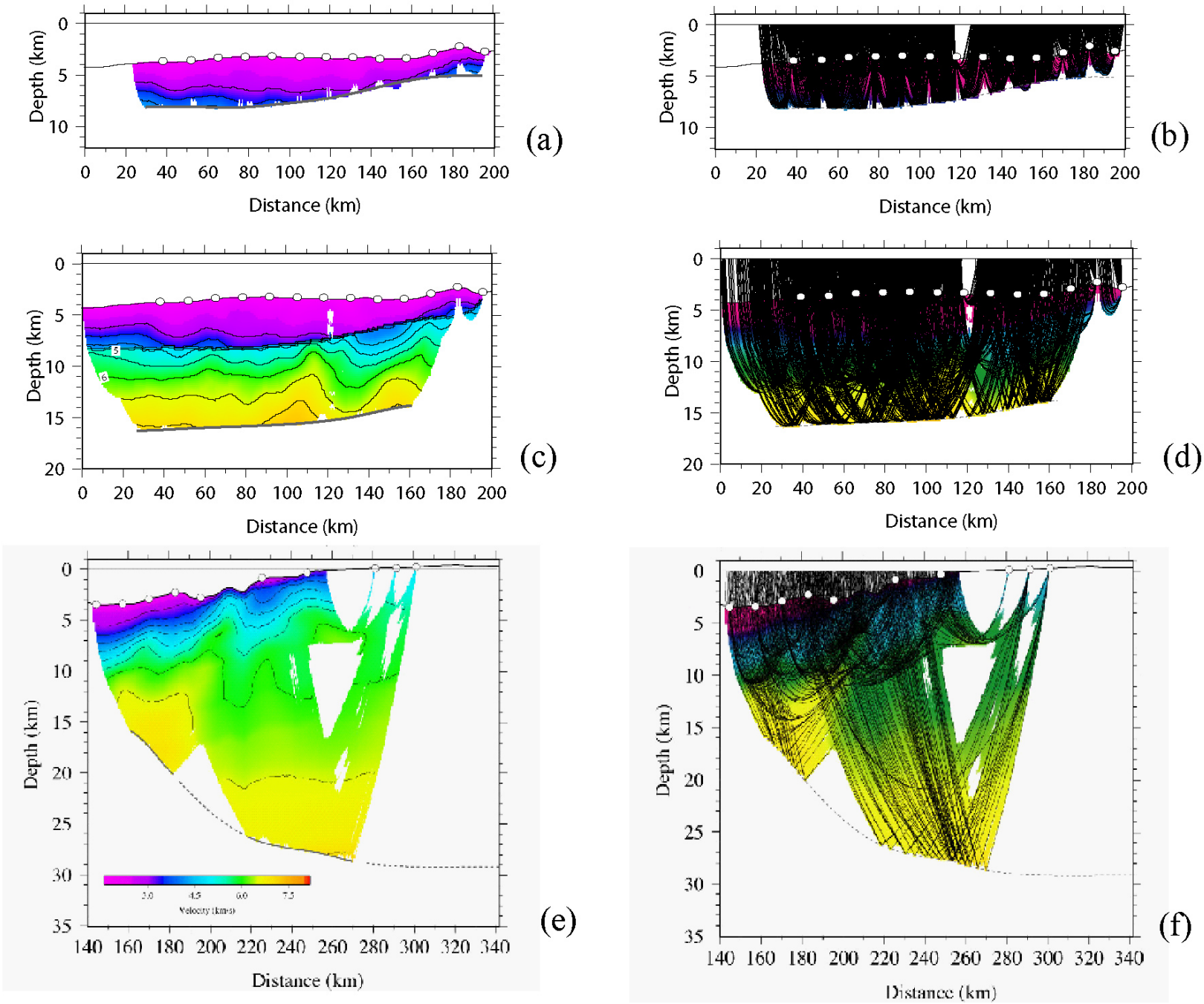
Depth (km)
Distance (km)
(a)
(b)
(c)
(d)
(e)
(f)

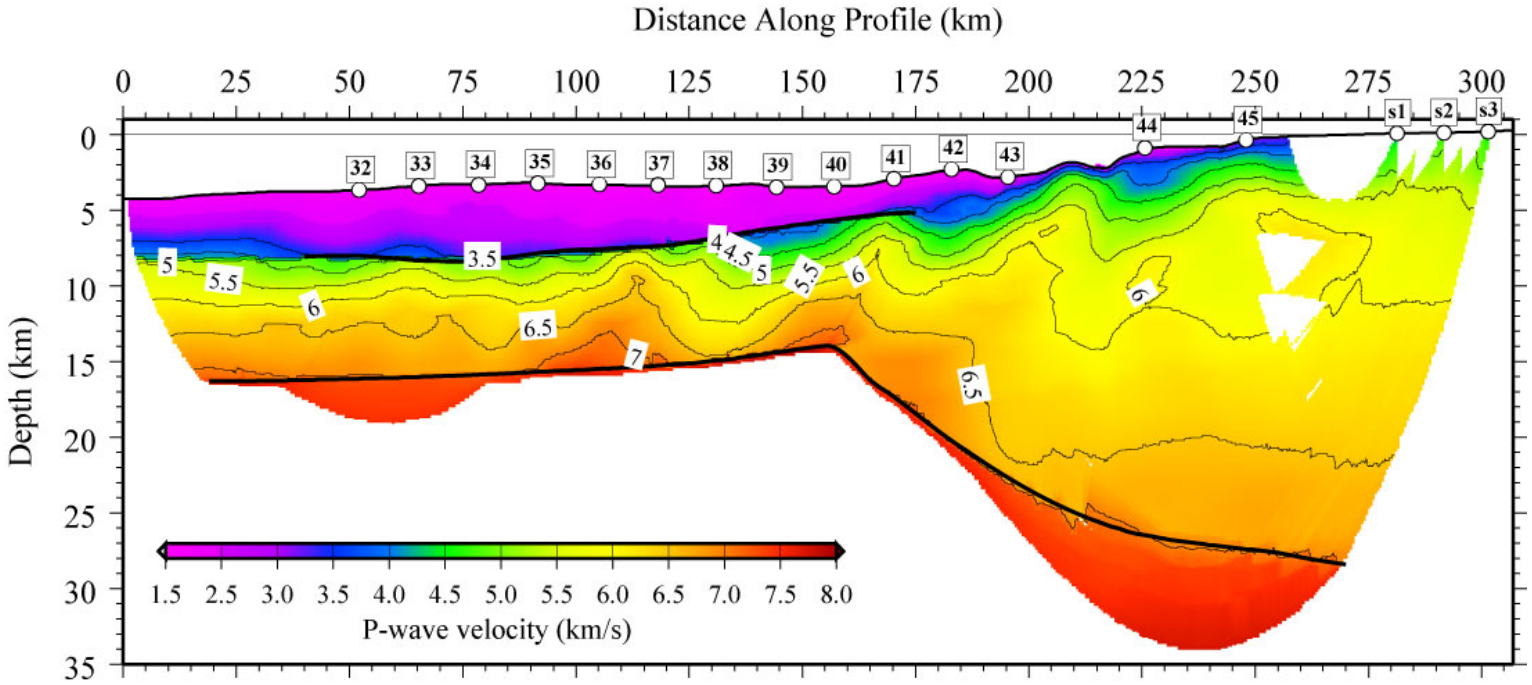
Distance Along Profile (km)
0
25
50
75
100
125
150
175
200
225
250
275
300
Depth (km)
0
5
10
15
20
25
30
35
32
33
34
35
36
37
38
39
40
41
42
43
44
45
s1
s2
s3
3.5
4
4.5
5
5.5
6
6.5
7
1.5
2.5
3.0
3.5
4.0
4.5
5.0
5.5
6.0
6.5
7.0
7.5
8.0
P-wave velocity (km/s)

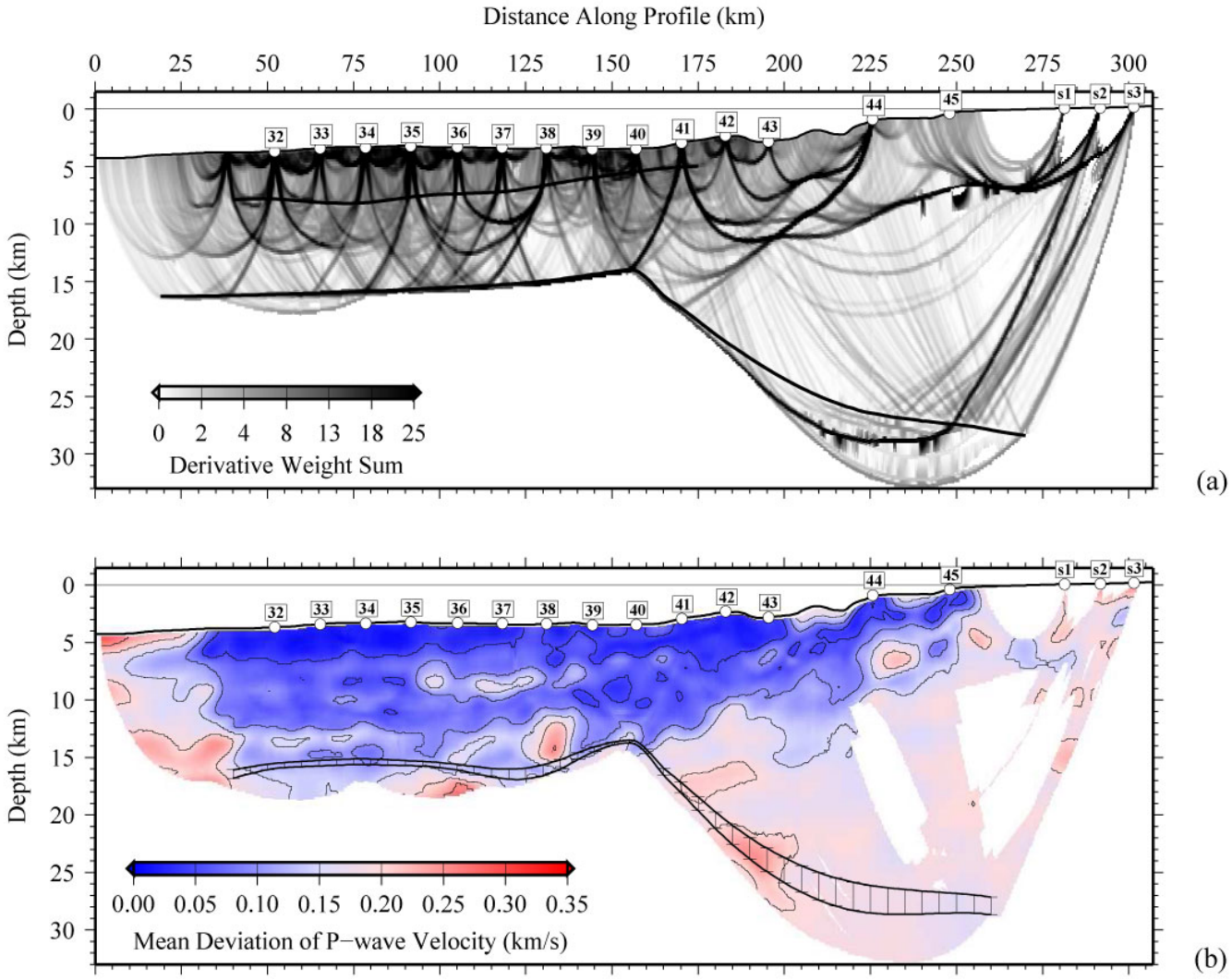
Distance Along Profile (km)
0 25 50 75 100 125 150 175 200 225 250 275 300
Depth (km)
0 5 10 15 20 25 30
32 33 34 35 36 37 38 39 40 41 42 43 44 45 s1 s2 s3
0 2 4 8 13 18 25
Derivative Weight Sum
(a)
0.00 0.05 0.10 0.15 0.20 0.25 0.30 0.35
Mean Deviation of P−wave Velocity (km/s)
(b)

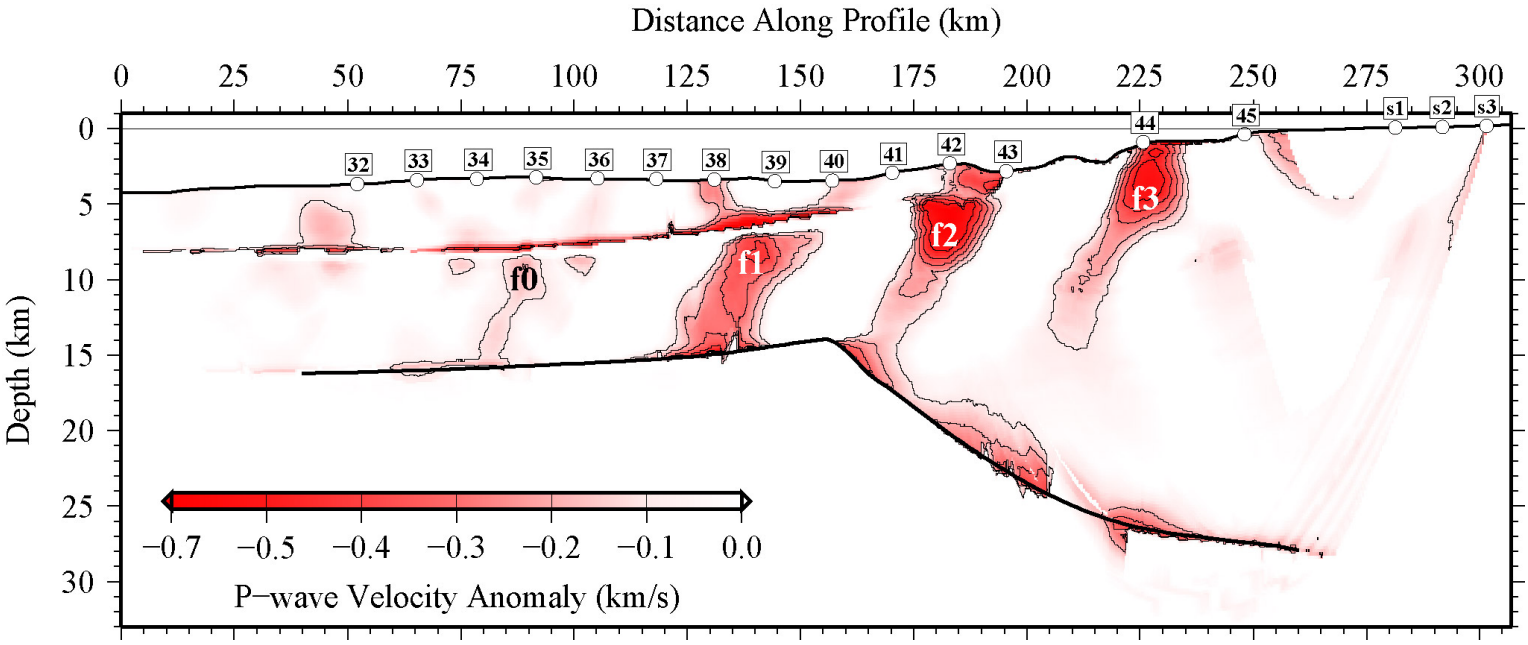
Distance Along Profile (km)
0
25
50
75
100
125
150
175
200
225
250
275
300
Depth (km)
0
5
10
15
20
25
30
32
33
34
35
36
37
38
39
40
41
42
43
44
45
s1
s2
s3
f0
f1
f2
f3
−0.7
−0.5
−0.4
−0.3
−0.2
−0.1
0.0
P−wave Velocity Anomaly (km/s)

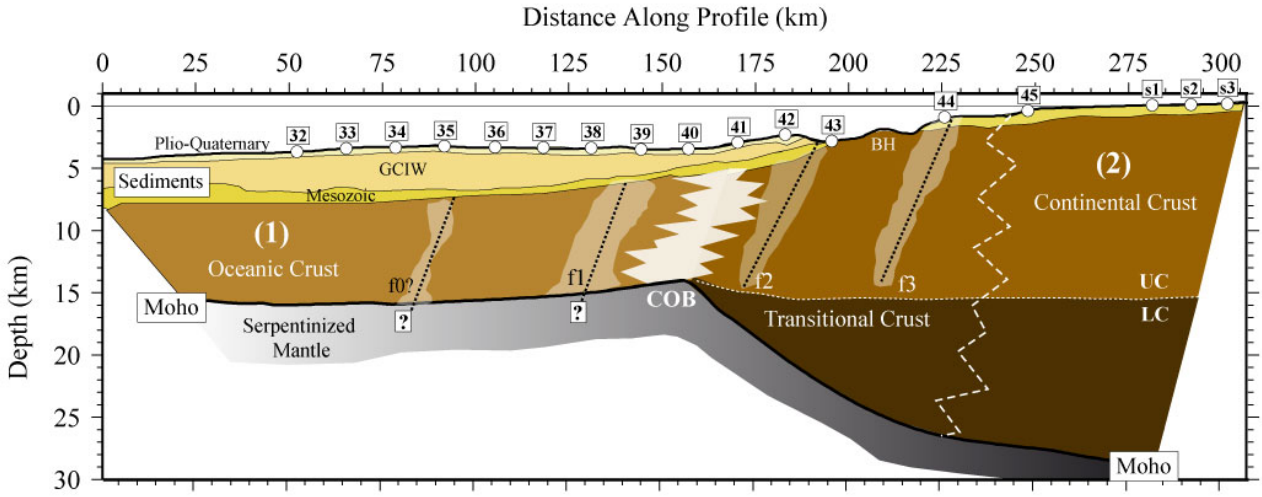
Distance Along Profile (km)
0
25
50
75
100
125
150
175
200
225
250
275
300
Depth (km)
0
5
10
15
20
25
30
32
33
34
35
36
37
38
39
40
41
42
43
44
45
s1
s2
s3
Plio-Quaternary
GCIW
Sediments
Mesozoic
(1)
Oceanic Crust
Moho
Serpentinized
Mantle
f0?
f1
f2
f3
?
?
COB
BH
(2)
Continental Crust
UC
LC
Transitional Crust
Moho

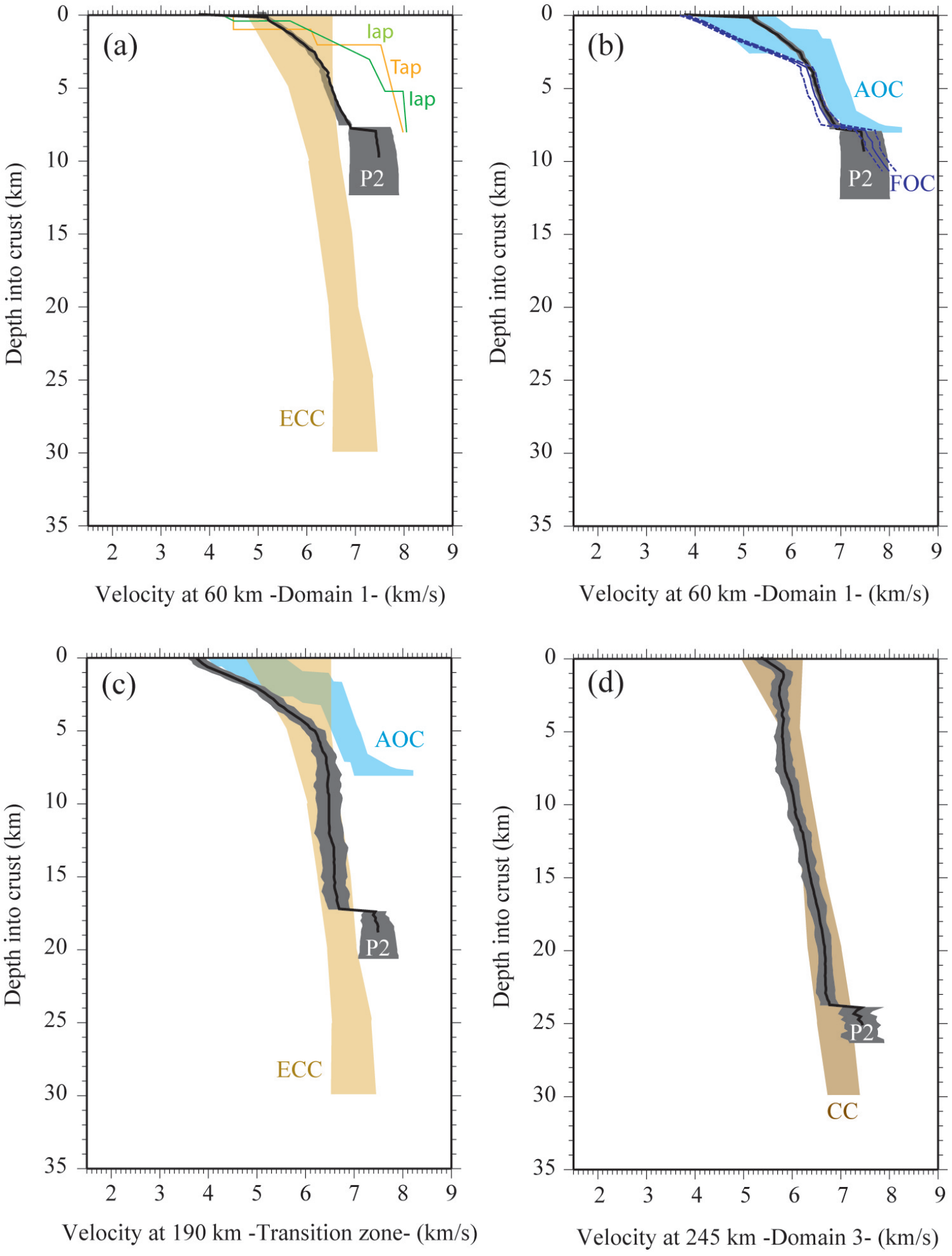
(a)
Iap
Tap
Iap
P2
ECC
Depth into crust (km)
Velocity at 60 km -Domain 1- (km/s)
(b)
AOC
P2
FOC
Depth into crust (km)
Velocity at 60 km -Domain 1- (km/s)
(c)
AOC
P2
ECC
Depth into crust (km)
Velocity at 190 km -Transition zone- (km/s)
(d)
P2
CC
Depth into crust (km)
Velocity at 245 km -Domain 3- (km/s)

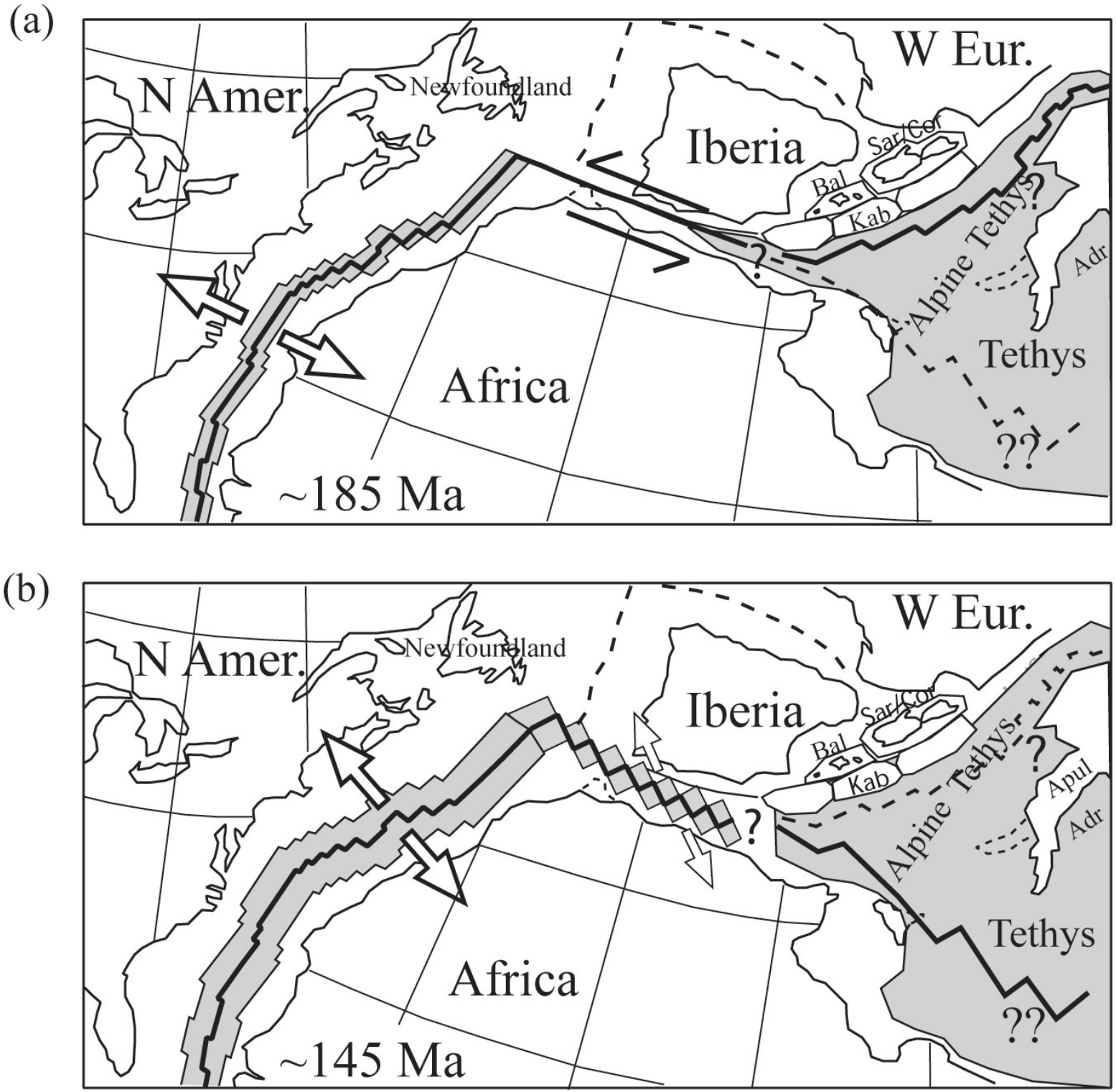
(a)
N Amer.
Newfoundland
W Eur.
Iberia
Sar/Cor
Bal
Kab
Alpine Tethys
Adr
Tethys
Africa
~185 Ma
(b)
N Amer.
Newfoundland
W Eur.
Iberia
Sar/Cor
Bal
Kab
Alpine Tethys
Apul
Adr
Tethys
Africa
~145 Ma